The finite temperature phase diagram of 2-flavour QCD with improved Wilson fermions

Dissertation

Zur Erlangung des Doktorgrades

Der Fakultät für Physik

der Universität Bielefeld

vorgelegt von

Manfred Oevers

Acknowledgements

An dieser Stelle möchte ich all jenen danken, die zur Entstehung dieser Arbeit beigetragen haben. Zunächts natürlich meinem Doktorvater Frithjof Karsch, der mir, meine nicht ungefährliche Neigung zum Abstrakten erkennend, dieses sehr konkrete Projekt vorschlug. Ich habe mich, wie schon bei meiner Diplomarbeit, bei ihm sehr gut aufgehoben gefühlt. Danken möchte ich auch Edwin Laermann, für seine berühmten glasklaren Kurzeinleitungen und den von Zeit zu Zeit nötigen Stups nach vorn. Ohne Peter Schmidts Vorarbeit und Mithilfe wäre der Hybrid Monte Carlo Code so schnell nicht fertiggeworden und die Auswertung nicht so ausgefeilt automatisiert. Ohne Burkhard Sturms Hilfe bei der Programmierung einiger Kernroutinen hätte es wohl auch noch länger gedauert. Ihm möchte ich auch für die vielen Diskussionen über Physik, Philosophie, Rheinländer und Westfalen danken, die wir in den 9 Jahren unseren gemeinsamen Studiums hatten. Sag mal Burkhard, surfst Du eigentlich? Nicht unerwähnt lassen möchte ich auch das Edinburgh Parallel Computing Centre. Mein dreimonatiger Aufenthalt im Rahmen des TMR Projekts TRACS (Training and Research on advanced Computing Systems) war sehr lehrreich und hat mir großen Spaß bereitet. Großes Glück hatte ich auch damit, daß Ian Barbour mich als Postdoc nach Glasgow holte und mir die Möglichkeit gab meine Arbeit dort aufzuschreiben. Um der Gefahr zu entgehen jemanden ungenannt zu lassen, möchte ich mich hier bei eben all den Ungenannten bedanken, die zu dem beitragen was Promovieren in Bielefeld ausmacht. Die Gespräche zwischen Tür und Angel, die Kaffeepause am Nachmittag, die geschlossenen Türen beim Daddeln, die offenen Türen unserer Dozenten, die vielen Workshops und Konferenzen an denen man im Laufe der Zeit teilgenommen hat, die gute Rechnerausstattung usw. Ausdrücklich erwähnen möchte ich noch unser Sekretariatsteam: Gudrun Eickmeyer, Karin Lacey und Susi von Reder. Danke für Eure gute Laune, Euren Service und Euren Spaß an der Arbeit.

Ich widme diese Arbeit meiner Familie; meinen Eltern Marita, Helmut und meinem Bruder Stephan. Ihr habt mich immer in meinem Streben unterstützt und mir die Wege freigemacht.

Contents

Chapter 1

INTRODUCTION

1.1 Motivation

Nuclear Matter is believed to undergo a phase transition from ordinary hadronic matter to a phase where quarks and gluons become deconfined. This belief is based on asymptotic freedom of QCD, the theory describing the strong interaction between quarks and gluons. This phase transition is not just of academic interest, since it has certainly taken place in the early universe according to current big bang theory. It will also become investigable at the Relativistic Heavy Ion Collider (RHIC) in Brookhaven and the Large Hadron Collider at CERN. In fact there are two true phase transitions characterized by an order parameter in two limits of QCD. When the quark masses are infinite, one has the deconfinement transition with the free energy of a static quark as the order parameter. When the quark masses are zero one has the chiral (symmetry restoring) phase transition with the vacuum expectation value of the quark anti-quark condensate as the order parameter. It is not yet clear if these transitions persist for physical quark masses. Lattice results indicate, that both transitions occur at the same temperature with one transition driving the other. This is the reason why one speaks of *the* QCD phase transition. At a phase transition point one typically has many length scales playing a role for the dynamics of the system. It is therefore often hard to find a suitable small expansion parameter for a perturbative treatment. In QCD for example one has three natural length scales given by the inverse temperature $1/T$, the electric screening mass $1/gT$ and the magnetic screening mass $1/g^2T$. The use of a nonperturbative approach, i.e. lattice QCD, is therefore advisable. Since thermal effects of massive particles are exponentially

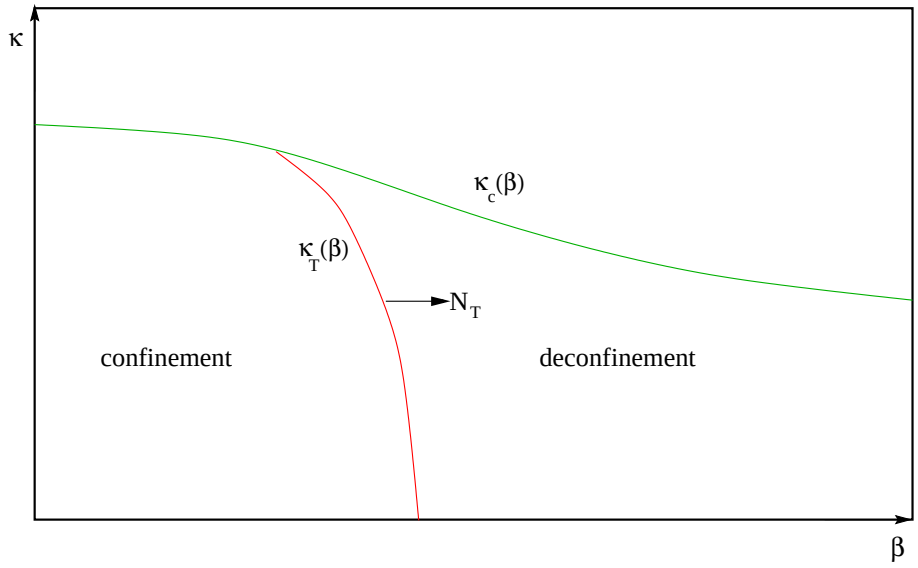

Figure 1.1: Expected phase diagram of 2 flavour QCD in the β-κ-plane

suppressed by their mass, the study of QCD with two light flavours is of particular phenomenological interest. Unfortunately the lattice has its own pitfalls, one of which is the nonexistence of an action which preserves chiral symmetry exactly for finite lattice spacing due to a general theorem [1]. Two popular discretisations exists and one has to check that the results obtained are consistent with each other. Most studies of QCD thermodynamics have employed staggered fermions, since they preserve a remnant chiral symmetry, which keeps the quark masses from acquiring an additive renormalisation, but which breaks the flavour symmetry at finite lattice spacing. The other discretisation due to Wilson preserves the flavour symmetry at the expense of breaking all chiral symmetries. This lack of chiral symmetry causes much conceptual and technical difficulties in numerical simulations and the physical interpretation of data. Before we turn to these problems let us discuss the physical expectations for the phase diagram of QCD as a function of temperature, quark mass and lattice spacing. On the lattice these parameters are mapped onto the temporal extent of the lattice N_τ, the hopping parameter κ and the inverse coupling β. This mapping is nonlinear, but some features of it are well known. The connection between inverse

coupling and the lattice spacing is such, that $a = 0$ for $\beta = \infty$ and vice versa. The inverse temperature is given by $N_\tau a$. Therefore the thermal line κ_T moves toward weaker coupling as N_τ increases. And finally, the line $\kappa = 0$ corresponds to infinite quark masses. Along this line, representing the pure gauge theory, a first order deconfinement phase transition is well established. This phase transition will extend into the phase diagram and the effect of the fermions will be to lower the transition temperature. The strength of the transition may soften and eventually turn into a rapid crossover rather than a true transition. For zero gauge coupling the critical hopping parameter κ_c at which the quark mass vanishes is known to be $\kappa_c = 1/8$. Since Wilson fermions break all chiral symmetries, this point is not protected from additive renormalisations and the critical line becomes β-dependent. This line corresponds to the chiral limit of QCD. One expects chiral symmetry to be broken spontaneously at zero temperature for phenomenological reasons and become restored at finite temperature. This chiral phase transition is believed to be of second order for two fermion flavours [2]. As we have mentioned before, both transitions coincide for intermediate quark masses, so one expects the deconfinement transition line to run into the critical line at some β_{ct}. Because of the absence of chiral symmetry for Wilson fermions, the definition of the critical line is ambiguous. One usually defines the critical line by the vanishing of the pion mass or quark mass at zero temperature. Where the quark mass is defined via an axial Ward identity [3]. Initial simulations [4] failed to find a crossing point down to $\beta = 3.5$ with the transition line running almost parallel to the critical line toward strong coupling. This raised the question whether it was possible to describe the confinement phase in the chiral limit with Wilson fermions. The issue was further investigated in [5] where the crossing point for 2 flavours at $N_\tau = 4$ was determined to be $\beta_{ct} \sim 3.9 - 4.0$. This was done by simulating along the critical line, defined by a vanishing pion mass at zero temperature. Coming from the high temperature side, where no singularity is seen across the critical line, the inverse coupling was lowered until such a singularity appeared in terms of a diverging number of CG-iterations. An investigation of how the position of the crossing point changed with increasing N_τ brought the disencouraging result, that to have $\beta_{ct} > 5.0$ one has to go to

$N_\tau > 18$! The transition was found to be continuous at β_{ct} as expected. This raises further expectations about the strength of the transition as the quark mass is increased from zero. The transition should soften as the quark mass increases, but should become stronger again when the quarks are heavy enough to recover the first order transition of the pure gauge system. Contrary to this expectation the MILC collaboration found [6] for $N_\tau = 4$ that the transition becomes once very strong and becomes weaker again at smaller κ. For $N_\tau = 6$ this intermediate transition even becomes first order. In summary this means that the finite temperature transition with Wilson quarks for small quark masses is plagued with lattice artifacts. In this study an improved action has been used whose derivation will be discussed in §(1.4). Recently a new view of the finite temperature phase diagram has emerged, which is based on the spontaneous breaking of parity and flavour symmetry. This proposal will be examined in Chapter 2. It is another goal of this study to test this proposal with improved actions.

1.2 Outline of this work

In the previous chapter we have tried to summarise the motivations leading to the research presented in this thesis. The remainder of Chapter 1 discusses some basic facts used throughout the thesis. We first discuss the chiral properties of Wilson fermions, as they play a central role in the analysis of the phase diagram. Then we discuss Symanzik's improvement program and its application to the fermionic and gluonic action. Chapter 2 discusses in some detail the phase diagram of QCD especially the proposal of Aoki and its application to finite temperature. Chapter 3 describes shortly the ideas of Monte Carlo integration used to evaluate the partition function, Markov processes to generate a desired probability distribution and the difficulties arising when fermionic degrees of freedom are added. The Pseudofermion method and the Hybrid Monte Carlo algorithm are described and equations of motion for the clover action derived. Chapter 4 discusses the results of our study. We will first present our findings and then argue for them from the results obtained from simulations on two different lattice sizes. Appendix A contains a short summary of how to quantize gauge and

fermion fields. This mainly serves to fix our notation. Appendix B lays down in detail the derivation of the equations of motion for the Hybrid Monte Carlo simulation.

1.3 Wilson fermions and chiral symmetry

In this section we want to discuss some of the chiral properties of Wilson fermions as they play a role in further discussions. Starting from the free action given in Equation (A.37) we want to determine the particle content of the theory. To identify the particles in the spectrum we study the poles of the fermion propagator in momentum space. We first rescale quark and anti-quark fields by a factor $a^3/\sqrt{2\kappa}$ where $\kappa = 1/2(am + 4r)$. With this new normalisation the free fermion action can be written as $S_f = \sum_x \bar{\psi}(x)\mathcal{M}_{x,y}\psi(y)$ with the fermion matrix

$$\mathcal{M}_{x,y} = \delta_{x,y} - \kappa \sum_{\mu} \delta_{x,y+\hat{\mu}}[r + \gamma_\mu] + \delta_{x,y-\hat{\mu}}[r - \gamma_\mu]. \tag{1.1}$$

We now go to momentum space, where we define the Fourier transform as

$$\psi(p) = \sum_x e^{-ipx}\psi(x) \quad \text{and} \quad \bar{\psi}(p) = \sum_x e^{ipx}\bar{\psi}(x). \tag{1.2}$$

Since the fermion matrix in momentum space only depends on one momentum, because of translation invariance, we get after factoring out of a momentum conserving delta function:

$$\mathcal{M}(p) = 1 - 2\kappa \sum_{\mu} r\cos(p_\mu) - i\gamma_\mu \sin(p_\mu). \tag{1.3}$$

The propagator is the inverse of the fermion matrix and it's poles give the particle content.

$$\Delta(p) \quad = \quad \left(1 - 2\kappa \sum_{\mu} r\cos(p_\mu) - i\gamma_\mu \sin(p_\mu)\right)^{-1}$$

$$
\begin{aligned}
&= \frac{1 - 2\kappa \sum_\mu r\cos(p_\mu) + i\gamma_\mu \sin(p_\mu)}{\left(1 - 2\kappa \sum_\mu r\cos(p_\mu)\right)^2 + 4\kappa \sum_\mu \sin^2(p_\mu)} \\
&= \frac{1}{2\kappa} \frac{\left(\frac{1}{2\kappa} - \sum_\mu r\cos(p_\mu)\right) + i\sum_\mu \gamma_\mu \sin(p_\mu)}{\left(\frac{1}{2\kappa} - \sum_\mu r\cos(p_\mu)\right)^2 + \sum_\mu \sin^2(p_\mu)}
\end{aligned} \tag{1.4}
$$

Now consider the case $r = 0$. For small a one can expand $\Delta(p)$ around $p_\mu = (0,0,0,0)$. The result is up to a normalisation factor the free fermion propagator in the continuum with $M = 1/2\kappa$

$$\Delta(p) \to \frac{M + i\not{p}}{M^2 + p^2}. \tag{1.5}$$

However the same result can also be obtained by expanding the lattice propagator around momenta p_μ which have one or more components in the other corner of the Brillouin zone. In fact all 16 corners of the Brillouin zone are equivalent. This is a consequence of the spectrum doubling symmetry [7]. This symmetry is generated by the following set of operators and products thereof:

$$T_0 = \mathbf{1}, T_\mu = \gamma_\mu\gamma_5(-1)^{x_\mu/a}. \tag{1.6}$$

It can be shown that these operators transform the physical fermion state near $p_\mu = (0,0,0,0)$ to doubler fermion states with momentum components in the far corner of the Brillouin zone, e.g.

$$(T_1\psi)(p_1,p_2,p_3,p_4) = \psi(p_1 + \pi/a, p_2, p_3, p_4). \tag{1.7}$$

Since this analysis only relied on the spinor structure of the theory it is clear, that the doublers will also exist if interactions are turned on. Then doublers can be pair produced by the gluons and that is why one is worried about them. In fact these additional states must appear. A chiral invariant regularisation of QCD cannot produce the axial anomaly in the continuum limit, due to Adlers

theorem. As shown in reference [7] the additional species have chiral charges such as to cancel the anomaly. For $r \neq 0$ the spectrum doubling symmetry is broken as is chiral symmetry. The contribution to the anomaly no longer cancels and produces the right anomaly, see again reference [7]. Let us now discuss the case $r \neq 0$. We analyse the behaviour of the term $M = 1/2\kappa - r\sum_\mu \cos(p_\mu)$ near the corners of the Brillouin zone. There are five different sets of momenta for which this term acts in a different way:

(i) $p = (0,0,0,0)$, $M = 1/2\kappa - 4r$

(ii) $p = (\pi/a,0,0,0)$ or $(0,\pi/a,0,0)$ etc., $M = 1/2\kappa - 2r$

(iii) $p = (\pi/a,\pi/a,0,0)$ or $p = (\pi/a,0,\pi/a,0)$ etc., $M = 1/2\kappa$

(iv) $p = (\pi/a,\pi/a,\pi/a,0)$ or $p = (\pi/a,\pi/a,0,\pi/a)$ etc., $M = 1/2\kappa + 2r$

(v) $p = (\pi/a,\pi/a,\pi/a,\pi/a)$. $M = 1/2\kappa + 4r$

If one now tunes κ to $\kappa_c = 1/8r$ the quark near $p = (0,0,0,0)$ becomes massless, whereas all other doublers get a mass of $O(1/a)$. In the continuum limit they decouple from the spectrum and one is left with one fermion flavour. The price we have to pay for this is of course the breaking of chiral symmetry. This implies that the value of $\kappa_c = 1/8r$ of the free theory is not protected by symmetry once we turn on interactions. The value for κ_c will depend on the gauge coupling and has therefore to be inferred from simulations. Note that one can choose κ such, that another set of doublers become massless, e.g. for $\kappa = 1/4r$ the doublers of set (ii) become massless and all others again have a mass of $O(1/a)$. This will become important in our discussion of the phase diagram in the next chapter.

1.4 The Symanzik improvement program

While studying the approach to the continuum limit for lattice ϕ^4-theory, Symanzik made the following important observation, see reference [8]. Suppose we start with a given lattice action S_L. The field theory described by this action is contained in the collection of all vertex function $\Gamma(p_1,p_2,\ldots,p_n;g^2,a)$. Symanzik

then introduced the concept of a local effective Lagrangian S_{eff} in terms of continuum fields, that would give the same vertex functions as S_L up to a certain order in the lattice spacing a.

$$S_{eff} = \int d^4x\{\mathcal{L}_0(x) + a\mathcal{L}_1(x) + a^2\mathcal{L}_2(x) + \ldots\}. \tag{1.8}$$

Where $\mathcal{L}_0$ is the continuum Lagrangian and $\mathcal{L}_k$ are a combination of local operators of dimension $4+k$ with the same symmetry as the lattice action. As the local effective Lagrangian is specific to the lattice action, one can use the freedom to choose the lattice action to speed up the approach to the continuum limit. The freedom one has to choose the lattice action is to add suitable linear combinations of irrelevant operators, i.e. lattice analogues of $\mathcal{L}_1$ etc., in such a way as to have $\mathcal{L}_1 = 0$ in the corresponding local effective Lagrangian. This program can then be carried out order by order in perturbation theory. Symanzik showed that all vertex functions can be thus improved in ϕ^4-theory. For lattice gauge theory no such proof exists, due to the fact that gauge dependent terms have to be added to the action at intermediate stages of the calculation. Lüscher and Weisz have therefore proposed a minimal improvement scheme by demanding improvement for on-shell quantities, hence the name on-shell improvement [9]. According to reference [10] no proof for the existence of an on-shell improved action has yet been given, but is tacitly assumed. One further ingredient to the derivation of a suitable on-shell improved action is, that given one on-shell improved action, others can be obtained from a local covariant isospectral transformation of the fields, where isospectral refers to the low-lying states. Such a transformation will in general change the coefficients of the operators in the original action. Operators whose coefficients can thus be varied are called redundant and their value can therefore be chosen for convenience. Let us now look at $O(a)$-improvement for gluons and fermions in particular.

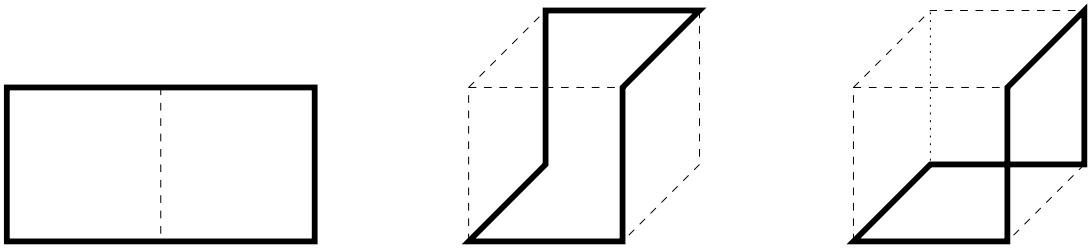

Figure 1.2: The three types of six link loops, figure taken from reference [11].

1.4.1 The $O(a)$-improvement of the gauge action

In the gluonic case there are no dimension 5 operators so the expansion of the local effective Lagrangian starts at $O(a^2)$. There are three dimension 6 operators

$$\begin{aligned} \mathcal{O}_1^{(6)} &= \sum_{\mu,\nu} \mathrm{Tr}\Big(D_\mu F_{\mu\nu} D_\mu F_{\mu\nu} \Big) \ , \\ \mathcal{O}_2^{(6)} &= \sum_{\mu,\nu,\rho} \mathrm{Tr}\Big(D_\mu F_{\nu\rho} D_\mu F_{\nu\rho} \Big) \ , \\ \mathcal{O}_3^{(6)} &= \sum_{\mu,\nu,\rho} \mathrm{Tr}\Big(D_\mu F_{\mu\rho} D_\nu F_{\nu\rho} \Big) \ . \end{aligned} \tag{1.9}$$

On the lattice this corresponds to loops with 6 links of which there are also only three, see Figure 1.2. Each of these loops has the expansion

$$\mathcal{L} \ = \ r^{(4)} \ \mathcal{O}^{(4)} + r_1^{(6)} \ \mathcal{O}_1^{(6)} + r_2^{(6)} \ \mathcal{O}_2^{(6)} + r_3^{(6)} \ \mathcal{O}_3^{(6)} + \dots \ , \tag{1.10}$$

Lüscher and Weisz have calculated these expansion coefficients at tree level, see reference [9]. The results are given in Table 1.4.1 The lattice action can now be written as

$$S_g \ = \ \frac{6}{g^2} \Big\{ c^{(4)}(g^2) \ \mathcal{L}^{(4)} + \sum_{i=1,3} c_i^{(6)}(g^2) \ \mathcal{L}_i^{(6)} \Big\} \tag{1.11}$$

Loop	$r^{(4)}$	$r_1^{(6)}$	$r_2^{(6)}$	$r_3^{(6)}$
$\mathcal{L}^{(4)}$	$-\frac{1}{4}$	$\frac{1}{24}$	0	0
$\mathcal{L}_1^{(6)}$	-2	$\frac{5}{6}$	0	0
$\mathcal{L}_2^{(6)}$	-2	$-\frac{1}{6}$	$\frac{1}{6}$	$\frac{1}{6}$
$\mathcal{L}_3^{(6)}$	-4	$\frac{1}{6}$	0	$\frac{1}{2}$

Table 1.1: The coefficients of the continuum operators of dimension 4 and 6 in the classical expansion of Wilson loops with 4 and 6 links.

From the results in Table 1.4.1 one can see, that tree level improvement can be obtained by choosing

$$c_0^{(4)} = \frac{5}{3}; \quad c_1^{(6)} = -\frac{1}{12}; \quad c_2^{(6)} = c_3^{(6)} = 0. \tag{1.12}$$

One can also improve the gauge action beyond tree level. This was carried out by Lüscher and Weisz in reference [12]. As it turns out, there are only two constraints one can get from demanding improvement of certain on-shell quantities. This is due to the fact that the operator $\mathcal{O}_3^{(6)}$ is redundant, as one can see from the field transformation

$$A_\mu \longrightarrow A_\mu + a^2 \frac{\epsilon}{2} \sum_\nu [D_\nu, F_{\mu\nu}]. \tag{1.13}$$

One can therefore set it to zero without affecting on-shell improvement to make the simulations easier. Since in this study we want to study the phase diagram at finite temperature, which at fixed temporal extent N_τ means large β, we expect tree level improvement to suffice.

1.4.2 The $O(a)$-improvement of the fermion action

In order to find an $O(a)$ improved fermion action let us first enumerate all operators up to dimension five.

dim3: $\mathcal{O}^3 = \bar{\psi}(x)\psi(x)$

dim4: $\mathcal{O}^4 = \bar{\psi}(x) \not{D} \psi(x)$

dim5: $\mathcal{O}_1^5 = \bar{\psi}(x)(D^2 - \frac{1}{2} i \sigma_{\mu\nu} F_{\mu\nu})\psi(x)$
$\mathcal{O}_2^5 = \bar{\psi}(x) \frac{1}{2} i \sigma_{\mu\nu} F_{\mu\nu} \psi(x)$

To translate these to the lattice, we define the following covariant derivatives:

$$\begin{aligned}
D_\mu^{right}\psi(x) &= \frac{1}{a}[U_\mu(x)\psi(x+\hat{\mu}) - \psi(x)] \\
D_\mu^{left}\psi(x) &= \frac{1}{a}[\psi(x) - U_\mu^\dagger(x)\psi(x-\hat{\mu})] \\
D_\mu^{L}\psi(x) &= \frac{1}{2}[D_\mu^{right} + D_\mu^{left}]\psi(x) \\
(D_\mu^2)^L\psi(x) &= \frac{1}{a}[D_\mu^{right} - D_\mu^{left}]\psi(x) \\
\Delta^L\psi(x) &= \sum_\mu (D_\mu^2)^L\psi(x)
\end{aligned} \tag{1.14}$$

To discretise $F_{\mu\nu}(x)$ we note that it can be obtained from the imaginary part of the plaquette. To preserve as much rotational symmetry as possible one averages over the four possible plaquettes starting at x the $\mu\nu$-plane:

$$\begin{aligned}
\mathcal{F}_{\mu\nu}(x) &= \frac{1}{8i}\big[U_\mu(x)U_\nu(x+\hat{\mu})U_\mu^\dagger(x+\hat{\nu})U_\nu^\dagger(x) \\
&+ U_\nu(x)U_\mu^\dagger(x+\hat{\nu}-\hat{\mu})U_\nu^\dagger(x-\hat{\mu})U_\mu(x-\hat{\mu}) \\
&+ U_\mu^\dagger(x-\hat{\mu})U_\nu^\dagger(x-\hat{\nu}-\hat{\mu})U_\mu(x-\hat{\nu}-\hat{\mu})U_\nu(x-\hat{\nu}) \\
&+ U_\nu^\dagger(x-\hat{\nu})U_\mu(x-\hat{\nu})U_\nu(x-\hat{\nu}+\hat{\mu})U_\mu^\dagger(x) \\
&- h.c.\big] \ .
\end{aligned} \tag{1.15}$$

With these definitions, the lattice operators can be written

$$\mathcal{O}_L^4 = \bar{\psi}(x)\gamma_\mu D_\mu^L \psi(x)$$

$$\begin{aligned}\mathcal{O}^5_{L,1} &= \bar{\psi}(x)(\Delta^L - \frac{i}{2a^2}\sigma_{\mu\nu}\mathcal{F}_{\mu\nu})\psi(x) \\ \mathcal{O}^5_{L,2} &= \bar{\psi}(x)\frac{i}{2a^2}\sigma_{\mu\nu}\mathcal{F}_{\mu\nu}\psi(x),\end{aligned} \tag{1.16}$$

and the lattice fermion action is given by

$$\begin{aligned}\mathcal{S}_f = \sum_x a^{-1}b_0(\beta, ma)\mathcal{O}^3_L(x) + b_1(\beta, ma)\mathcal{O}^4_L(x) + \\ a\ b_2(\beta, ma)\mathcal{O}^5_{L,1}(x) + a\ b_3(\beta, ma)\mathcal{O}^5_{L,2}(x).\end{aligned} \tag{1.17}$$

Since tree level improvement is consistent with classical improvement, requiring the vanishing of all corrections to the continuum action to $O(a)$ in the small a expansion of the lattice action gives a tree level Symanzik improved fermion action. This condition requires for the coefficients $b_i(\beta = 0, ma)$

$$b_0(0, ma) = ma, \quad b_1(0, ma) = 1, \quad b_2(0, ma) = b_3(0, ma) = 0, \tag{1.18}$$

i.e. the naive fermion action is tree level $O(a)$ improved. The next step is to use an isospectral transformations to remove the doublers from the physical spectrum. Since the doublers involve high momentum modes we are allowed to change their properties. Using an isospectral transformation makes sure we do not spoil $O(a)$ improvement as we remove the doublers. The transformation is given by:

$$\begin{aligned}\psi(x) &\longrightarrow \psi(x) + \epsilon_1 \not{D}\psi(x) \\ \bar{\psi}(x) &\longrightarrow \bar{\psi}(x) + \epsilon_2 \not{D}\bar{\psi}(x),\end{aligned} \tag{1.19}$$

It renders the operator $\mathcal{O}^5_1(x)$ redundant and one can add it with an arbitrary coefficient. The coefficient of the operator $\mathcal{O}^5_2(x)$ has to be determined perturbatively, but at tree level its value is $b_3(0, ma) = 0$. The Alpha collaboration have invented a way to determine this coefficient nonperturbatively, but the results were not yet available when this study was begun. We therefore used the tree

level value $c_{sw} = 1$. The action used in this study is hence given as $S = S_g + S_f$, where S_g and S_f are given in a graphical representation below.

$$S_g = \frac{6}{g^2} \sum_{x,\mu>\nu} \frac{5}{3} \left(1 - \frac{1}{N} \mathrm{ReTr} \right)_{\mu\nu}(x) - \frac{1}{6} \left(1 - \frac{1}{2N} \mathrm{ReTr} \left(\right)_{\mu\nu}(x) + \left(\right)_{\mu\nu}(x) \right) \right) \tag{1.20}$$

$$S_f = \frac{1}{2\kappa} \sum_{x,y} \bar{\Psi}(x) \Big\{ \left(\mathbf{1} - \frac{\kappa}{2} \sum_{\mu,\nu} \mathrm{Im} \right)_{\mu\nu} (x)\, \sigma_{\mu\nu} \Big) \delta_{x,y} - \kappa \sum_{\mu} \Big[(\mathbf{1} - \gamma_\mu)\, \delta_{x+\hat{\mu},y} \longrightarrow_{\mu}(x) + (\mathbf{1} + \gamma_\mu)\, \delta_{x-\hat{\mu},y} \longleftarrow_{\mu}(y) \Big] \Big\} \Psi(y) \tag{1.21}$$

Chapter 2

The Finite Temperature Phase Diagram of 2-flavour QCD

2.1 The early understanding

The first analysis of the phase structure of lattice QCD is reference [13]. Kawamoto studied the singularity structure of the chiral condensate, because it has the same radius of convergence (in κ) as the fermion propagator and can easily be extended to the fermion gauge coupled system. He found a singularity in $\langle\bar{\psi}\psi\rangle$ at $\kappa_c = 1/4$ in the strong coupling and large N limit, where N is the number of colours. This value is lowered as Ng^2 is lowered from infinity. He also found a singularity at $\kappa_c = 1/8$ in the weak coupling limit, whose value is increased as the gauge interaction is taken into account. From this observation Kawamoto conjectured, that a line of singularities in $\langle\bar{\psi}\psi\rangle$, connecting the singularities in the strong and weak coupling limit, exists. The region where $\kappa < \kappa_c(\beta)$ is the physical region. On the line $\kappa_c(\beta)$ the pion mass vanishes, and for $\kappa > \kappa_c(\beta)$ the pion mass becomes imaginary. In the weak coupling region also the quark mass vanishes along the critical line with $M_\pi^2 \approx m_q$. This is one of the conditions to hold for a theory with spontaneous breakdown of chiral symmetry. Another condition is the vanishing of the pion-pion scattering amplitude at zero momentum in the chiral limit. This however is not satisfied on the critical line in the strong coupling limit. Although the critical line has conventionally been interpreted as the line along which at zero temperature chiral symmetry is spontaneously broken, Kawamoto's results in fact indicate, that this interpretation is not straightforward.

2.2 Aoki's Proposal

In 1984 Aoki challenged this picture for a number of reasons [14]. If there is a line dividing the β - κ plane into two phases, what is the order parameter to distinguish the two phases? How can the pion become a tachyon, when the action of QCD has physical positivity? Is a spontaneous breakdown of chiral symmetry possible with only one critical line? Aoki went on to propose a new phase diagram for 1 flavour QCD with Wilson fermions:

- There exist 5 continuum limits for four dimensional QCD corresponding to different regions in momentum space where different sets of doublers become massless: (i) $p = (0,0,0,0)$, (ii) $p = (\pi/a,0,0,0)$ or $(0,\pi/a,0,0)$ etc., (iii) $p = (\pi/a,\pi/a,0,0)$ or $p = (\pi/a,0,\pi/a,0)$ etc., (iv) $p = (\pi/a,\pi/a,\pi/a,0)$ or $p = (\pi/a,\pi/a,0,\pi/a)$ etc. and (v) $p = (0,0,0,0)$. The true continuum limit is of course (i). A pair of critical lines on which the π-meson mass vanishes is associated whith each continuum limit

- There exist regions in the $\beta - \kappa$ plane, where the $\left\langle \bar{\psi} i\gamma_5 \psi \right\rangle = 0$ vacuum becomes unstable and the true vacuum has $\left\langle \bar{\psi} i\gamma_5 \psi \right\rangle \neq 0$. The transition between these phases occurs at the critical lines mentioned above.

- In the strong coupling limit only two critical lines exist where the π-meson mass vanishes. Therefore no separation of the doublers occurs.

- At intermediate coupling, new critical lines emerge, that separate the five regions in momentum space.

The properties of this phase diagram are drawn from two sources. One is the 2 dimensional lattice Gross-Neveu model formulated with the Wilson action in the large N limit, where N is the number of colours. In this limit one can solve the G-N model analytically and finds the above picture verified. Calculating the pion mass near the critical point M_c one obtains the PCAC-like relation $m_\pi^2 \approx (M - M_c)$, without recourse to chiral symmetry. The other source is strongly coupled QCD, also in the large N limit. Calculating the effective potential in this limit one finds,

that in addition to the conventional phase with $\langle \bar{\psi} i\gamma_5 \psi \rangle = 0$ there exists a phase with $\langle \bar{\psi} i\gamma_5 \psi \rangle \neq 0$ for $0 \leq M^2 \leq 4$, where $M = m_q a + 4r = 1/2\kappa$ is the mass parameter. Calculating the pion mass one finds, that its mass vanishes only at the transition point. This shows, that the pion is the massless mode connected with the parity breaking phase transition. These results are unchanged, when one includes the first corrections in β in the large N limit [15]. Investigating the case of two flavours again at $\beta = 0$ in the large N limit, one finds two different kinds of vacua due to an accidental symmetry of the solution to the saddle point equation:

$$\langle \bar{\psi} i\gamma_5 \mathbf{1} \psi \rangle \neq 0 \quad \text{and} \quad \langle \bar{\psi} \mathrm{i}\gamma_5 \boldsymbol{\tau_3} \psi \rangle = 0 \tag{2.1}$$

$$\langle \bar{\psi} i\gamma_5 \mathbf{1} \psi \rangle = 0 \quad \text{and} \quad \langle \bar{\psi} \mathrm{i}\gamma_5 \boldsymbol{\tau_3} \psi \rangle \neq 0 \tag{2.2}$$

The vacuum of Equation (2.1) breaks only parity invariance, whereas the vacuum of Equation (2.2) breaks both the flavour symmetry and the parity invariance. The true vacuum can be found using the strong coupling expansion which removes the degeneracy between the vacua. It turns out, that Equation (2.2) is the true vacuum, i.e. both parity and flavour symmetry are spontaneously broken for $M^2 \leq 4$ in the strong coupling expansion. Calculating the meson masses one finds, that the neutral pion π_0 becomes massless at the phase transition, as do the charged pions $\pi_\pm$ due to flavour symmetry. The η meson stays massive at the transition which solves the $U(1)$ problem on the lattice. In the parity flavour broken phase 2 Goldstone bosons must appear which are the charged pions. However the neutral pion becomes only massless at the transition point [16]. The approach to the critical line will be governed by some critical exponent, so one expects $m_\pi^2 \sim (\kappa_c - \kappa)^{2\nu}$. Since low energy properties of pions can be described by an effective 4-dimensional scalar field theory, one expects the phase transition to be mean field like up to logarithmic corrections and therefore $\nu = 1/2$, reproducing the PCAC relation $m_\pi^2 \propto m_q a$, where the quark mass is defined as $m_q a = (\frac{1}{2\kappa_c} - \frac{1}{2\kappa})$. Using chiral ward identities, one can define a current quark

mass via [3]

$$2m_q^{WI} \equiv \frac{\sum_{x,y,t}\langle \nabla_3 \bar{\psi}\gamma_5\gamma_3\psi(x_\mu)\cdot\bar{\psi}\gamma_5\psi(0)\rangle}{\sum_{x,y,t}\langle \bar{\psi}\gamma_5\psi(x_\mu)\cdot\bar{\psi}\gamma_5\psi(0)\rangle}. \tag{2.3}$$

This quantity is not a tunable parameter and the existence of a chiral limit is not ensured. However the above scenario explains how the theory obtains such a limit.

2.3 An effective Lagrangian analysis

In reference [17] the phase structure of 2-flavour QCD close to the continuum limit was studied using an effective continuum Lagrangian whose long range behaviour can be analysed using a chiral Lagrangian. The effective continuum Lagrangian is the same we encountered in the Symanzik improvement program

$$\mathcal{L}_{\text{eff}} = \mathcal{L}_{\text{g}} + \bar{\psi}(\not{D} + m)\psi + b_1 a\bar{\psi}i\sigma_{\mu\nu}F_{\mu\nu}\psi \ , \tag{2.4}$$

where $\mathcal{L}_g$ is the gluon Lagrangian and terms of $O(a^2)$ have been dropped. Writing down an effective chiral Lagrangian leads to

$$\mathcal{L}_\chi = \frac{f_\pi^2}{4}\,\mathsf{Tr}\,\left(\partial^\mu\Sigma^\dagger\partial_\mu\Sigma\right) + \mathcal{V}_\chi\,. \tag{2.5}$$

The first term is invariant under $SU(2)_L \times SU(2)_R$ chiral rotations, as is the effective continuum Lagrangian without mass and Pauli term. The second part $\mathcal{V}_\chi$ contains the symmetry breaking terms up to second order in m:

$$\mathcal{V}_\chi = -\frac{c_1}{4}\mathsf{Tr}\left(\Sigma+\Sigma^\dagger\right) + \frac{c_2}{16}\left\{\mathsf{Tr}\left(\Sigma+\Sigma^\dagger\right)\right\}^2 \ . \tag{2.6}$$

Since the Pauli term transforms under chiral rotations in the same way as the mass term, its effects can be absorbed into the coefficients c_1 and c_2. Dimensional analysis then tells us that

$$c_1 \sim m\Lambda^3 + a\Lambda^5\ ,\ c_2 \sim m^2\Lambda^2 + ma\Lambda^4 + a^2\Lambda^6\,, \tag{2.7}$$

Where Λ is an abbreviation for Λ_{QCD}. As one reduces the mass at fixed lattice spacing, one enters a region where the two coefficients become comparable in magnitude and the competition between the two terms can lead to spontaneous parity and flavour breaking. For masses $m \sim a\Lambda^2$ discretization effects become important and the mass at which c_1 vanishes is shiftet from $m = 0$ to $m' = 0$ with $m' = m - a\Lambda^2$. When this shifted mass is of $O(a^2)$, i.e. $am' = (a\Lambda)^3$, the size of the coefficients becomes comparable. Writing

$$\Sigma = A + i\mathbf{B} \cdot \boldsymbol{\sigma} \text{ with } A^2 + \mathbf{B}^2 = 1, \tag{2.8}$$

the potential becomes

$$\mathcal{V}_\chi = -c_1 A + c_2 A^2 \,, \tag{2.9}$$

having a minimum/maximum at $\epsilon = c_1/2c_2$. Denoting the vacuum state by $\Sigma_0 = A_0 + i\mathbf{B}_0 \cdot \boldsymbol{\sigma}$, one sees that a nonzero $\mathbf{B}_0$ breaks the flavour symmetry to $U(1)$. A nonzero $\mathbf{B}_0$ can only occur for $|A_0|$ less than one. The sign of c_2 distinguishes two different scenarios. For $c_2 < 0$ the minimum of the potential is attained for $A_0 = \pm 1$. Hence flavour symmetry is not broken, but the pions do not become massless either. For $c_2 > 0$ the minimum of the potential lies at ϵ, hence if $|\epsilon| > 1$ the vacuum is $A_0 = \pm 1$, but for $|\epsilon| < 1$ the vacuum is $A_0 = \epsilon$ and flavour symmetry becomes spontaneously broken. Since $\epsilon \sim m'/(a^2\Lambda^3)$ with $m' = m - a\Lambda^2$, one sees explicitly, that the Aoki phase has width $\Delta m_0 \sim a\Delta m' \sim (a\Lambda)^3$. This analysis cannot predict the sign of c_2 and stays essentially unaltered for the improved case. The sign of c_2 can however change when one goes to the improved case, so the existence of an Aoki phase for improved Wilson fermions is an open question.

2.4 Application to finite temperature

The application of these ideas to the phase structure at finite temperature was put forward in reference [18]. They defined the critical line at finite temperature $\kappa_c(\beta)$ by the vanishing of the pion screening mass. This definition makes contact

with the standard definition at zero temperature and is a natural extension to finite temperature. The question then arises how this line is related to the finite temperature transition line $\kappa_T(\beta)$, defined for definitiveness sake by the peak in the susceptibility of the chiral condensate. One would expect the two lines to meet on the following physical ground. Moving along the critical line towards increasing β increases the temperature. Since one expects the restoration of chiral symmetry at high temperature, one should find a point where the chiral condensate drops to zero and the corresponding susceptibility has a peak, i.e. one should cross the $\kappa_T(\beta)$ line. Initial simulations failed to find clear signals of such a behaviour. As reviewed in reference [19] the finite temperature line runs almost parallel to the critical line, defined by the vanishing of the pion mass at zero temperature, towards strong coupling, raising the question whether the two lines meet at all. Subsequent simulations determined the crossing point by running along the zero temperature critical line towards strong coupling until the number of conjugate gradient iterations diverged signaling the appearance of a massless mode, namely the pion, in the spectrum. Using the one plaquette action for the gluons and the Wilson action for the fermions, the crossing point was determined to lie deep in the strong coupling region at $\beta_{ct} = 3.9{-}4.0$. The shift of this crossing point with N_τ was studied and it was estimated that $N_\tau \gtrsim 18$ would be needed to have the crossing point in the week coupling region. Another way out is the use of improved action for the gauge field, which is pursued in this study. Aoki, Ukawa and Umemura then analysed the two dimensional Gross-Neveu model formulated with the Wilson action at finite temperature. Except for confinement, this model shares many important features with QCD, as there are asymptotic freedom, spontaneous breakdown of chiral symmetry and its restoration at finite temperature. In the large N limit, the pion mass is analytically calculable and the result is given in Figure 2.1. The main feature is the fact that the three cusps retract from the weak coupling limit for finite temporal lattice sizes, forming a continuous line which shifts toward strong coupling as N_τ decreases. The position of the critical line obviously depends on N_τ, but only slightly for large N_τ. For QCD the number of cusps will increase to five because of the different dimensionality and the line of the finite temperature transition will appear. To

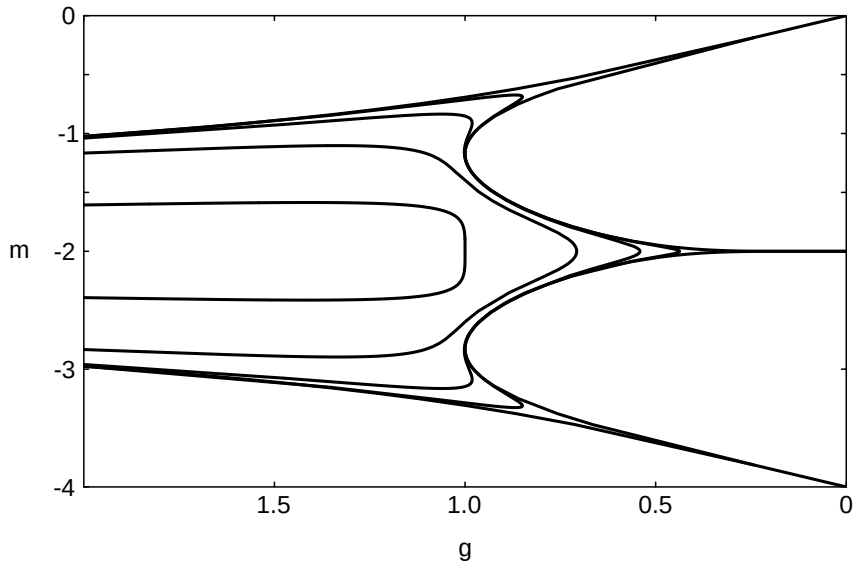

Figure 2.1: Critical lines for the lattice Gross-Neveu model on the (g,m) plane. Temporal lattice sizes are $N_t = 2, 4, 6, 16$ and ∞ from inside to outside. Figure taken from reference [18].

define a unique point of the chiral phase transition the thermal line has to cross the critical line. The thermal line can however not extend into the parity-flavour breaking phase, since massless pions exist in this phase. Therefore the line κ_T cannot cross the line κ_c for finite N_τ, but may at most touch it. This means, that the region close to the critical line belongs to the low temperature phase even after it turns back toward strong coupling. This means, that the thermal line should extend past the tip of the cusp to separate the high temperature region from the low temperature region. The absence of the critical line at weak enough coupling naturally explains that physical quantities vary smoothly across the zero temperature critical line. This line $\kappa_c(T = 0)$ is absent from the point of view of the finite temperature partition function, i.e. it is not a line of thermodynamic singularities. Another line enters the phase diagram namely the line of vanishing current quark mass defined by Equation (2.3). This line extends from the point $(\beta, \kappa) = (\infty, \frac{1}{8})$ into the phase diagram. It runs towards the tip of the cusp of the Aoki phase and runs alongside it towards the point $(\beta, \kappa) = (0, \frac{1}{4})$. This is so,

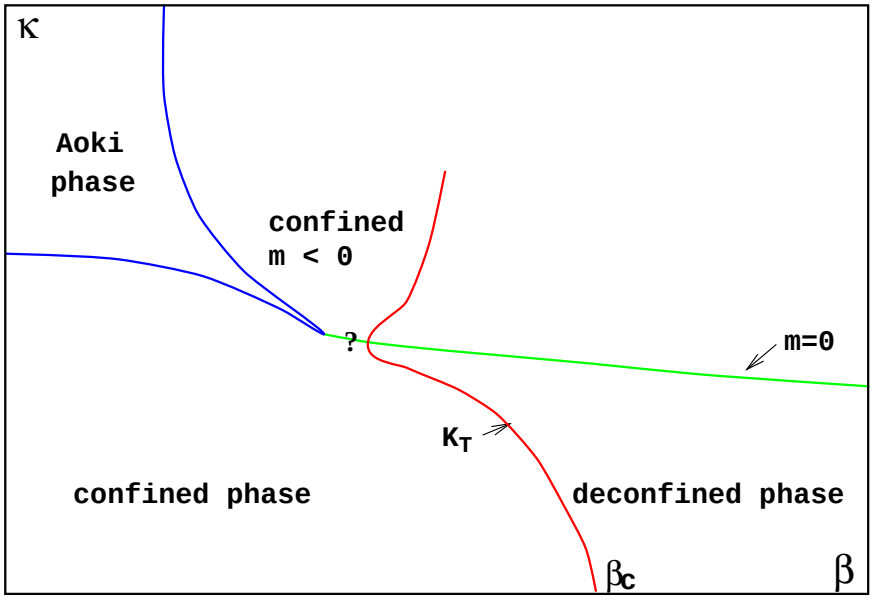

Figure 2.2: Phase diagram for 2-flavour QCD with improved Wilson fermions in the $\beta - \kappa$ plane.

because at zero temperature the critical line coincides with the $m_q = 0$ line and the critical line at zero temperature smoothly develops into the zero temperature critical line. If the thermal line $\kappa_T(\beta)$ runs past the cusp of the Aoki phase and does not touch the Aoki phase, there will be room for a phase transition, probably first order, from a confined phase with positive quark mass to a confined phase with negative quark mass, see reference [20]. Creutz also points out, that the thermal line is expected to bounce back towards weak coupling as one crosses the $m_q = 0$ line, because in the continuum the sign of the mass term is irrelevant for 2-flavour QCD. Since most features of the phase diagram rely on generic features of Wilson fermions, namely the way doublers are treated at the expense of chiral symmetry, one expects these features to hold when an improved action is used. Beware however the caveat mentioned at the end of §(2.3) This is the reason for using the Sheikoleslami-Wohlert action for the fermions. We want to study whether the phase diagram with improved actions also exhibits a phase structure containing an Aoki phase.

Chapter 3

Simulating Lattice QCD

3.1 Monte Carlo Integration and Markov processes

In a computer simulation of Euclidean field theory one is interested in expectation values of operators Ω which depend on some fundamental field Φ whose dynamic is governed by an action $\mathcal{S}(\Phi)$. The expectation value is then calculated as

$$\langle \Omega \rangle = \frac{1}{Z} \int [d\Phi] e^{-\mathcal{S}(\Phi)}, \tag{3.1}$$

Where $[d\Phi]$ is the path integral measure, Z is the partition function chosen such that $\langle 1 \rangle = 1$. The main idea of Monte Carlo integration is now to generate a sequence of field configurations $(\Phi_1, \Phi_1, \ldots, \Phi_t, \ldots, \Phi_N)$ each chosen from the probability distribution

$$P(\Phi_t)[d\Phi_t] = \frac{1}{Z} e^{-\mathcal{S}(\Phi)} [d\Phi_t]. \tag{3.2}$$

Measuring the observable on each of these configurations and taking the average will give

$$\langle \Omega \rangle = \lim_{N \to \infty} \bar{\Omega} = \lim_{N \to \infty} \frac{1}{N} \sum_{t=1}^{N} \Omega(\Phi_t). \tag{3.3}$$

For large N the distribution of $\bar{\Omega}$ will be Gaussian with standard deviation $\sigma = \sigma_\Omega / \sqrt{N}$, where $\sigma_\Omega = \sqrt{\langle \Omega^2 \rangle - \langle \Omega \rangle^2}$. To create the desired probability distribution one makes use of Markov processes. A Markov process is a stochastic

procedure, that given a configuration Φ_i generates a new configuration Φ_f with some transition probability $P(\Phi_i \to \Phi_f)$. The new configuration therefore depends only on its predecessor. A Markov process is called ergodic if and only if

$$\alpha = \inf_{\Phi_i, \Phi_f} P(\Phi_i \to \Phi_f) > 0 \tag{3.4}$$

Given a probability distribution $Q(\Phi)$ on the space of configurations, application of the Markov process will change this distribution unless it is a fixed point, i.e.

$$\int [d\Phi_i] Q(\Phi_i) P(\Phi_i \to \Phi_f) = Q(\Phi_f). \tag{3.5}$$

The remarkable property of *ergodic* Markov processes is that for any such process there exists a unique fixed point Q. The distribution of configurations will converge to this fixed point no matter what the starting configuration was and this convergence is exponential. To construct an ergodic Markov process that has the desired probability distribution $Q(\Phi) = e^{-\mathcal{S}(\Phi)}/Z$ as its fixed point, the transition probability has to satisfy another condition known as *detailed balance*:

$$Q(\Phi_i) P(\Phi_i \to \Phi_f) = P(\Phi_f \to \Phi_i) Q(\Phi_f). \tag{3.6}$$

It should be noted, that this is a sufficient but not a necessary condition for the transition probability. One simple way of implementing detailed balance is the Metropolis algorithm:

$$P(\Phi_i \to \Phi_f) = \min \left[1, \frac{Q(\Phi_f)}{Q(\Phi_i)} \right] \tag{3.7}$$

If the action $\mathcal{S}(\Phi)$ is local, we can build up an ergodic Markov process by a product of non ergodic steps, involving an update of one degree of freedom at a time. Since the action is local, the evaluation of $Q(\Phi_f)/Q(\Phi_i)$ at each step is cheap. As soon as the action becomes nonlocal, this method becomes infeasible

and other methods have to be used. Unfortunately this is exactly the case, when fermions enter the game:

$$\begin{aligned} Q(\bar{\psi},\psi,U) &= \frac{1}{Z}\exp\{-\mathcal{S}(\bar{\psi},\psi,U)\}\ [d\bar{\psi}][d\psi][dU] \\ &= \frac{1}{Z}\exp\{-\mathcal{S}_g(U)-\bar{\psi}\mathcal{M}(U)\psi\}\ [d\bar{\psi}][d\psi][dU] \\ &= \frac{1}{Z}\det(\mathcal{M}(U))\exp\{-\mathcal{S}_g(U)\}\ [dU]. \end{aligned} \tag{3.8}$$

Integrating out the fermions thus leaves us with an effective action for the gauge fields that is highly nonlocal. How one can simulate such a system with reasonable efficiency is the subject of the next section.

3.2 Pseudofermions and Hybrid Monte Carlo

In any Metropolis accept/reject step one would have to calculate the ratio of two determinants, which is an operation cubic in the lattice volume, regardless of how many entries of the matrix are changed. One way to circumvent the evaluation of a determinant is by trading it in for the inverse of a matrix by using a well known formula for Gaussian integrals.

$$\det\mathcal{M} = \int d\Phi d\Phi^* e^{-\Phi^*\mathcal{M}^{-1}\Phi}, \tag{3.9}$$

which applies if the real part of all eigenvalues of $\mathcal{M}$ is larger than zero. This is not true for the fermion matrix of a single flavour. But we can make use of the following property of the fermion matrix of Wilson fermions:

$$\gamma_5\mathcal{M}\gamma_5 = \mathcal{M}^\dagger. \tag{3.10}$$

This implies that the determinant of $\mathcal{M}$ is real. Since every additional flavour of mass degenerate fermions adds another power of the fermion determinant into the path integral, we can use Equation (3.10) to double the number of fermions

and make Equation (3.9) work:

$$(\det \mathcal{M})^2 = \det \mathcal{M}^\dagger \det \mathcal{M} = \det(\mathcal{M}^\dagger \mathcal{M}) = \int d\Phi d\Phi^* e^{-\Phi^*(\mathcal{M}^\dagger \mathcal{M})^{-1}\Phi}. \quad (3.11)$$

This is the pseudofermion method. Since the pseudofermions appear in a Gaussian integral, it is easy to do the Monte Carlo integration of them. Choosing η from a Gaussian distribution $P(\eta) \sim \exp(-\eta^*\eta)$ and setting $\Phi = \mathcal{M}^\dagger \eta$ will ensure that Φ has the distribution required by Equation (3.11). What remains is to find a Markov process, that evolves the gauge fields. The effective action for the gauge fields now involves the inverse of the fermion matrix. This matrix becomes ill conditioned when there is a massless mode in the spectrum, i.e. when the pion becomes massless. This means that even a small change in the gauge fields will give rise to a large change of the pseudofermionic energy and the acceptance rate would be very small. The idea of the Hybrid Monte Carlo (HMC) algorithm is therefore to evolve the system globally in a judiciously chosen way and then decide about the acceptance of these changes as a whole [21]. We introduce additional degrees of freedom which are canonically conjugate momenta to the gauge degrees of freedom. We define a fictitious Hamiltonian

$$\mathcal{H} = \tfrac{1}{2} \sum_{x,\mu} \mathrm{Tr}\ \pi_\mu^2(x) + \mathcal{S}_g(U) + \Phi^*(\mathcal{M}^\dagger \mathcal{M})^{-1}\Phi. \quad (3.12)$$

Creating field configurations $\{\pi, U, \Phi\}$ with a Boltzmann weight given by $\mathcal{H}$, namely $Q(\pi, U, \Phi) \sim \exp(-\mathcal{H})$ will produce the right correlation functions for gauge and fermion fields, since the fictitious momenta can be integrated out. The HMC algorithm alternates two Markov processes which both have $Q(\pi, U, \Phi)$ as a fixed point, but neither of which is ergodic by itself.

The first step is a refreshment of the momenta chosen from a Gaussian distribution. The second step is to evolve the gauge fields and momenta, using Hamilton's equations of motion, along a molecular dynamics trajectory which keeps the energy $\mathcal{H}$ constant. Since one has to discretise these equations of motion in order to integrate Hamiton's equations, one can not preserve the energy. Adding a

Metropolis accept/reject step at the end of each trajectory will then ensure detailed balance. The conventional way to derive the equations of motion was given in reference [22]. To preserve U as an element of $SU(N)$ the equations of motion have to take the form

$$\dot{U} = i\pi U, \tag{3.13}$$

where π has to be an element of the Lie algebra of $SU(N)$. The equations of motion for π are fixed by the requirement that $\mathcal{H}$ should stay constant along the trajectory. A mathematically more satisfying treatment is given in reference [23]. There the formalism for classical mechanics on an arbitrary compact Lie group $\mathcal{G}$ is developed and applied to the case of HMC. The result is

$$\dot{\pi} = -T\left[\frac{\partial \mathcal{S}}{\partial U}U\right], \tag{3.14}$$

where T is the projector onto the Lie algebra of $\mathcal{G}$. For the case of $SU(N)$ this amounts to projecting out the traceless antihermitian part. For the case of 2-flavour QCD this will give

$$\begin{aligned}\frac{\partial \mathcal{S}}{\partial U} &= \frac{\partial \mathcal{S}_g}{\partial U} + \Phi^* \frac{\partial}{\partial U}(\mathcal{M}^\dagger \mathcal{M})^{-1}\Phi \\ &= \frac{\partial \mathcal{S}_g}{\partial U} + [(\mathcal{M}^\dagger \mathcal{M})^{-1}\Phi]^* \frac{\partial}{\partial U}(\mathcal{M}^\dagger \mathcal{M})[(\mathcal{M}^\dagger \mathcal{M})^{-1}\Phi].\end{aligned} \tag{3.15}$$

The computational bottleneck is of course the computation of $[(\mathcal{M}^\dagger \mathcal{M})^{-1}\Phi]$. To discretise these equations one has to find a scheme that is both reversible and area preserving. The simplest one is the *Leapfrog* scheme. Evolve $U(0)$ half a time step to $U(\frac{1}{2}dt)$ using

$$U(\tfrac{1}{2}dt) = U(0) + \dot{U}(\tfrac{1}{2}dt)dt, \tag{3.16}$$

then perform the leapfrog steps

$$\pi(t+dt) = \pi(t) + \dot{\pi}(t+\tfrac{1}{2}dt)dt \tag{3.17}$$

$$U(t+\tfrac{1}{2}dt) = U(t-\tfrac{1}{2}dt) + \dot{U}(t)dt \tag{3.18}$$

and close the trajectory by another half step for the U fields. The detailed calculation of the equations of motion for our kind of action are derived in Appendix A.

Chapter 4

Numerical Results with improved Wilson fermions

This chapter describes the results obtained through numerical simulation of two flavour QCD with improved Wilson fermions on lattices of size $8^3 \times 4$ and $12^2 \times 24 \times 4$. Using routines to invert the fermion matrix and the correlator code written by Peter Schmidt for a quenched spectroscopy project, a Hybrid Monte Carlo code was set up together with Peter Schmidt and Burkhard Sturm. This code in its final version comprised 104 routines making up 19700 lines of (commented) code, which ran for about 200000 CPU hours on the Cray T3E at the Höchstleistungs Rechen Zentrum in Juelich, Germany.

4.1 Overview of results

Before we delve into the wealth of data, we want to summarise our findings on the phase diagram. Figure 4.1 shows the location of the thermal line and the critical line in the β-κ plane. For $\beta = 2.8$ we have found two κ values at which the quark mass vanishes indicating the existence of the Aoki phase. Furthermore the system shows confined behaviour up to about $\kappa = 0.2$ when the finite temperature transition slowly sets in. This means that the thermal line runs past the tip of the cusp of the Aoki phase and does not turn back toward weak coupling as put forward in reference [20]. In fact we see no sign of a second thermal line at large κ up to $\kappa = 0.33$. At $\beta = 3.0$ the gap between the two vanishing points of the quark mass is no longer seen and the critical line almost coincides with the finite temperature transition line. At $\beta = 3.1$ one crosses the thermal line before the critical line when κ is increased. We follow both lines up to $\beta = 3.75$ observing,

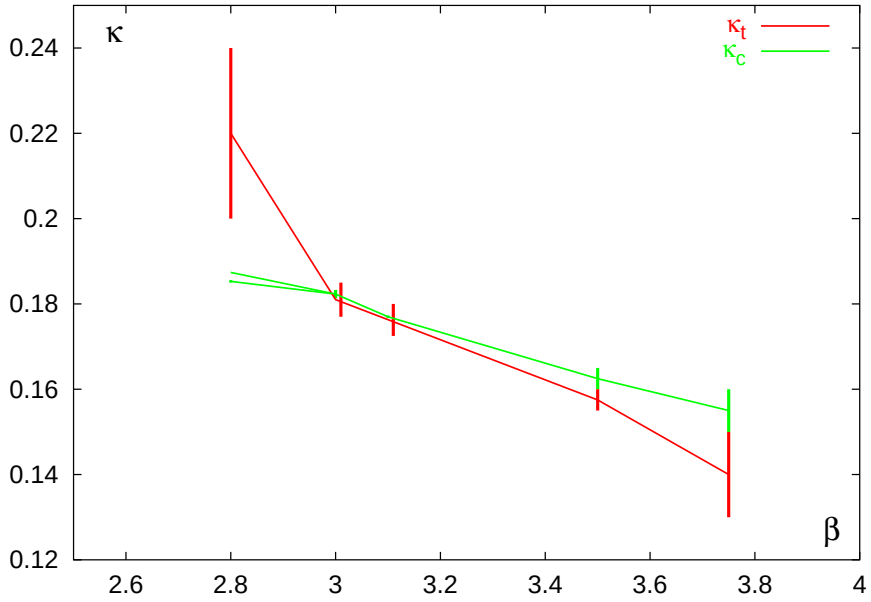

Figure 4.1: Results for the location of the critical line and thermal line in the β-κ plane for two flavours of improved Wilson fermions.

that they stay quite close together, as seen in earlier studies with the standard Wilson action. For the thermal line the vertical bars indicate the approximate range over which the transition takes place. For the critical line we have except for $\beta = 2.8$ and 3.1 only data from the small lattice size, where an accurate extraction of large distance behaviour of propagators is not possible. Yet there is still a pronounced change in the behaviour, when the quark mass changes sign. This information can then be used to locate the critical line. The vertical bars for the critical line are drawn between the points where the quark mass changes sign. For $\beta = 2.8$ and 3.1, where we have data from the larger lattice, the error of the fit result is shown.

In the following sections we will discuss in detail the results that corroborate this picture, but before we can do this we have to define the observables.

4.2 Definition of the observables

Since we are ultimately interested in the finite temperature phase transition in the chiral limit of two flavour QCD, we need a set of observables, that is sensitive to both the chiral and thermal behaviour of the system. The simplest observable sensitive to chiral properties is the **pion norm** defined by

$$\Pi = \frac{1}{4N_\sigma^3 N_\tau} \cdot \mathrm{tr}\ \left[\mathcal{M}^{-1}\gamma_5\mathcal{M}^{-1}\gamma_5\right], \tag{4.1}$$

which is just the integrated pion propagator. For light quark masses the pion norm is proportional to the inverse pion mass squared, $\Pi \sim 1/m_\pi^2$. It can therefore be used on a smaller lattice to asses the proximity to the chiral limit, where accurate information on the pion mass is not available.
The **pion screening mass** is extracted from the exponential decay of the spatial pseudoscalar correlator, projected onto zero momentum in all orthogonal directions

$$\langle\pi(z)\pi(0)\rangle = \sum_{x,y,t}\langle\bar{\psi}\gamma_5\psi(x_\mu)\cdot\bar{\psi}\gamma_5\psi(0)\rangle. \tag{4.2}$$

The connection between the screening mass m and the correlator is given by

$$C(z) = 2A\exp(-mN_z/2)\cosh(m(N_z/2-z)) \tag{4.3}$$

which is valid for large enough z.
Another quantity of prime interest is the quark mass. By a careful analysis of chiral ward identities reference [3] shows how to suitably define physical quantities in order to get the correct chiral continuum limit. Following their prescription, we define the **quark mass** as

$$2m_q = Z_A\frac{\sum_{x,y,t}\langle\nabla_3\bar{\psi}\gamma_5\gamma_3\psi(x_\mu)\cdot\bar{\psi}\gamma_5\psi(0)\rangle}{\sum_{x,y,t}\langle\bar{\psi}\gamma_5\psi(x_\mu)\cdot\bar{\psi}\gamma_5\psi(0)\rangle}. \tag{4.4}$$

Z_A is the renormalisation constant of the axial current, which we set to its tree level value, which for our normalisation of the fermion fields is $1/(2\kappa)^2$. This is strictly speaking not correct, but we are mainly interested in the location of the line of vanishing quark mass for which the difference does not matter. The renormalisation constant can however be obtained from an analysis of three point functions.

In the chiral limit of QCD the **chiral condensate** becomes an order parameter for the finite temperature chiral phase transition. At low temperature we expect chiral symmetry to be spontaneously broken and therefore the chiral condensate to extrapolate to a nonzero value in the chiral limit. In the symmetry restored phase the chiral condensate should vanish as the the quark mass goes to zero. For Wilson fermions a properly subtracted definition of the order parameter has to be used to cancel the contact terms arising from the Wilson term. The proper definition was again given in reference [3]:

$$\langle\bar{\psi}\psi\rangle_{sub} = 2m_q \cdot Z_A \cdot \sum_{x,y,z,t} \langle\pi(x_\mu)\pi(0)\rangle \tag{4.5}$$

When the quarks are infinitely heavy, full QCD reduces to pure gauge theory. Here the deconfinement phase transition is related to the spontaneous breakdown of the $Z(N_c)$ center symmetry. The order parameter for this phase transition is the **Polyakov-loop**, whose expectation value can be related to the partition function of a static quark coupled to the gauge fields. The Polyakov loop is defined by

$$L = \frac{1}{N_\sigma^3} \sum_{\vec{x}} \mathrm{tr} \prod_{t=1}^{N_\tau} U_4(\vec{x}, t). \tag{4.6}$$

We have first carried out a preparatory study on the small lattice of size $8^3 \times 4$ to get an idea about the location of the finite temperature transition line and the location of the cusp of the Aoki phase if it existed. We have used the Polyakov loop and the pion norm to map out the phase diagram. We had also measured the relevant correlators to determine the pion mass and the quark mass, but could

not extract clear and unambiguous signals from them. We simulated the system for $\beta = 2.8, 3.0, 3.1, 3.5$ and 3.75 at various values of κ. Once the phase diagram was approximately known, we used a larger lattice of $12^2 \times 24 \times 4$ at two β values, namely $\beta = 2.8$ and 3.1, to corroborate our findings, check finite size effects and extract pion and quark masses. With hindsight it turned out that to a certain extent one could use the calculated correlators on the smaller lattice to extract viable information. We will deliberate on this in the appropriate section.

4.3 Results for the pion norm

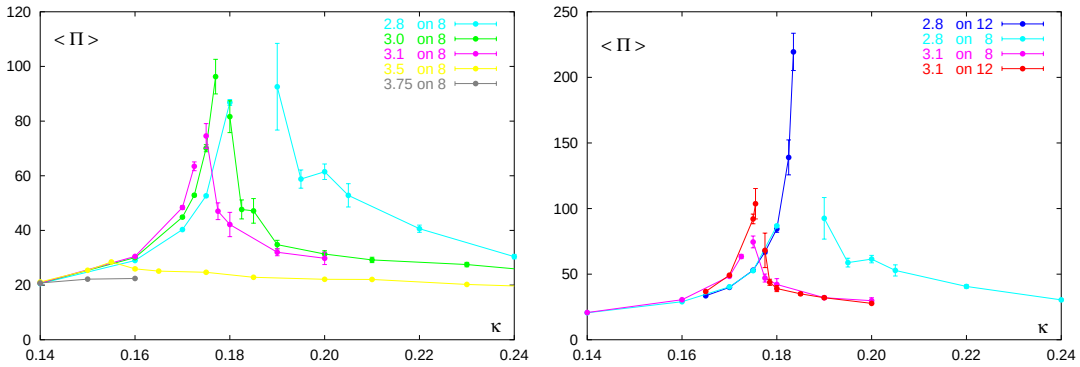

Figure 4.2: Left: The pion norm as a function of κ on the $8^3 \times 4$ lattice for different β values. Right: Similarly data from the $12^2 \times 24 \times 4$ lattice together with corresponding data from the smaller lattice to asses finite size effects. N.B.: note the difference in scale.

Figure 4.2 shows the results for the pion norm. We expect the pion norm as a function of κ to develop a peak that increases as we decrease β. This peak should turn into a singularity as one hits the tip of the Aoki phase. Lowering β further, the singularity should split up into two branches and and leave a gap. As we can see from Figure 4.2, one can identify this behaviour in our data. At $\beta = 3.75$ the pion norm does not develop any peak and there is no sign of a proximity to the Aoki phase. At $\beta = 3.5$ the pion norm develops a small peak whose location coincides with that of the deconfinement transition, see §(4.4). At $\beta = 3.1$ one sees a clear signal for a diverging pion norm. As one decreases β further to

β	2.8	3.0	3.1
κ_c	0.1859(3)	0.1823(10)	0.1800(5)

Table 4.1: Critical hopping parameters extracted from the pion norm.

$\beta = 3.0$ the apparent gap between the two branches of the developing divergence becomes wider. We will argue below, that one can identify two critical lines for $\beta = 2.8$, which can be understood by the existence of Aoki's phase. As mentioned above one expects the pion norm to be inversely proportional to the squared pion mass. Employing the partial conservation of the axial current the squared pion mass is proportional to the quark mass. For the quark mass one has in turn the relation

$$m_q \sim \frac{1}{2}\left(\frac{1}{\kappa_c} - \frac{1}{\kappa}\right), \tag{4.7}$$

which is valid as an equality in the weak coupling limit where $\kappa_c = 1/8$. At finite β one has to use the appropriate value for $\kappa_c(\beta)$ and the proportionality constant becomes unequal a half. One can therefore extract a $\kappa_c(\beta)$ from fitting $1/\Pi$ linearly in $1/\kappa$. The results are shown in Table 4.1; except for $\beta = 3.0$ we used the data from the larger of the two lattice sizes in the analysis. The fit was only performed approaching the critical line from below, because $1/\Pi$ showed a strong curvature when plotted as a function of $1/\kappa$ for the larger values of κ. In the next section we will argue, that for $\beta = 3.1$ the data are not consistent with the proposition that the pion becomes massless. For $\beta = 3.0$ we cannot decide the issue, so we are left with only $\beta = 2.8$ where the existence of the Aoki phase can be established.

4.4 Results for the Polyakov loop

Figure 4.3 shows the results for the Polyakov loop. As one can infer from the right plot, the finite size effects are not very large for the two β-values where data from both lattices exist. We therefore assume the finite size effects for the

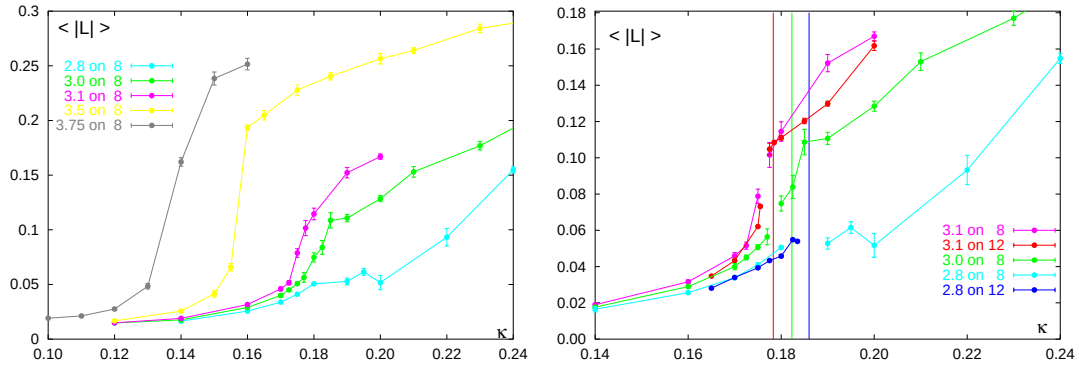

Figure 4.3: Left: The Polyakov loop as a function of κ on the $8^3 \times 4$ lattice for different β values. Right: Similarly data from the $12^2 \times 24 \times 4$ lattice together with corresponding data from the smaller lattice to asses finite size effects, vertical lines are critical values of κ as extracted from the pion norm. N.B.: note the difference in scale.

other β-values to be small as well and use all data to infer the phase diagram. As explained in §(1.1) one expects the critical temperature of the phase transition to decrease, when the mass of the quarks is lowered. This means, that the location of the transition is shifted to larger κ for smaller β. This is clearly exhibited by the data. For $\beta = 3.75$ the transition is quite strong as expected for large quark masses where the first order phase transition of the pure gauge system is still important. The transition takes place between $\kappa = 0.13$ and $\kappa = 0.15$. These values quoted here are the basis for the vertical bars given for the thermal line in Figure 4.1. For $\beta = 3.5$ the transition is still quite strong taking place between $\kappa = 0.155$ and $\kappa = 0.16$. The jump in the value of the Polyakov loop however is smaller than for $\beta = 3.75$ as expected. For $\beta = 3.1$ the transition is even weaker and happens between $\kappa = 0.1725$ and $\kappa = 0.18$. This means that the pion cannot become massless at κ=0.18 which was the fit result from the pion norm. The system is already in the high temperature regime where the fit would suggest the pion to become massless. This means that for β=3.1 one crosses the thermal line before the critical line. This will be further supported by the analysis of the results for the quark mass and the pion mass as presented below. For $\beta = 3.0$

where the finite temperature phase transition takes place between $\kappa = 0.177$ and $\kappa = 0.185$, the point where the fit from the pion norm would predict a massless pion is right where the transition happens. This indicates that the critical line and the thermal line come very close around $\beta = 3.0$. For $\beta = 2.8$ there is no problem with the interpretation, that the pion becomes massless for some value of the hopping parameter. Though the Polyakov loop increases with κ it remains small and shows no transition behaviour as one approaches the critical line. On the other side of the apparent singularity the Polyakov loop slowly rises and shows transient behavior between $\kappa = 0.20$ and $\kappa = 0.24$. This means that the thermal line runs past the tip of the cusp of the Aoki phase continuing toward strong coupling. The transition however is weaker and more spread out than for larger values of β.

4.5 Results for the pion mass

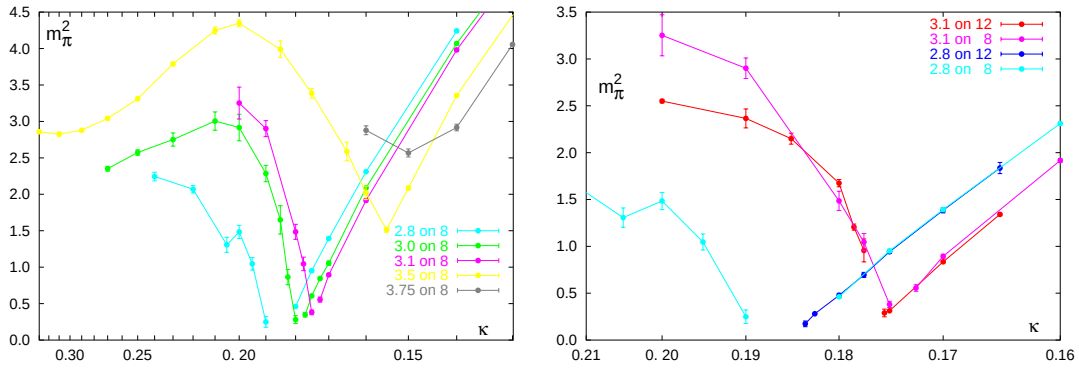

Figure 4.4: Left: Value of the second z-slice of the effective mass plot of the pion correlator squared as a function of $1/\kappa$ for the $8^3 \times 4$ lattice. Right: Fitted pion mass squared as a function of $1/\kappa$ from the $12^2 \times 24 \times 4$ lattice together with data from the smaller lattice as on the left

We have measured the pion-pion correlator on both lattice sizes, but only on the larger lattice is it possible to extract a mass from an exponential fit. We have however analysed the correlator also on the smaller lattice and produced an effective mass plot, i.e. plotting the average ratio of the correlator of two

consecutive time slices. If we compare the second time slice of such an effective mass plot on the smaller lattice with the fitted mass from the larger lattice at corresponding values of β and κ we find a surprisingly good agreement, as can be seen from the right part of Figure 4.4. We hence also plot this quantity as the pion mass for the other β-values on the smaller lattice, to see whether the results fit into the overall picture. We have to keep in mind though, that these values have to be taken with a grain of salt. Let us now discuss the pion mass on the smaller lattice. For $\beta = 3.75$ the pion stays heavy. The pion mass decreases with increasing κ, but becomes heavier again once we cross the transition region. For $\beta = 3.5$ this behaviour becomes even more pronounced, with the minimum value of the pion mass occurring right at the finite temperature phase transition. Furthermore this minimum value is lower than for $\beta = 3.75$ which fits well with our finding that the critical line and the thermal line come closer together as one decreases β. Another interesting feature for this β-value is that the pion after getting heavier after the finite temperature transition becomes lighter again at even higher values of κ. This seems to indicate the proximity to another cusp of the Aoki phase as we expect in total five cusps to develop. For $\beta = 3.1$ we can compare the pion mass on the smaller lattice with the properly extracted one from the larger lattice. As one can see from Figure 4.4 they agree quite well for κ's in the low temperature phase. In the high temperature phase the agreement is not so good, which might be explained by the fact, that in the high temperature phase there is strictly speaking no pion. This means, that what we measure is in fact the propagator of two quarks propagating in the medium. In this case finite size effects play an important role. We should hence be very careful in interpreting the pion mass data in the high temperature phase. At $\beta = 3.1$ we clearly see that the data are not compatible with the assumption that the pion mass becomes zero. At $\beta = 3.0$ the situation is less clear cut also because we have no data from the larger lattice. The minimum value of the pion mass is lower than for $\beta = 3.1$ but not consistent with zero. For larger κ-values we see a similar behaviour as for $\beta = 3.5$, namely the pion mass drops again. Finally at $\beta = 2.8$ there is evidence that the pion becomes massless. The two branches of the plot can be extrapolated to yield two different values for κ_c which leave a small gap.

β	2.8	2.8
κ_c	0.188(1)	0.1859(1)

Table 4.2: Results for the two critical hopping parameters at $\beta = 2.8$ extrapolated from the pion mass.

The result of a linear extrapolation is shown in Table 4.2. The errors are quite large which comes from the fact, that the data show quite some curvature as a function of $1/\kappa$. This might be a result of the left out renormalisation factor. On the other hand the argument for a linear behaviour of the pion mass squared as a function of $1/\kappa$ is drawn from PCAC ideas, which due to Aoki are not really applicable here. We also have no problem that these κ-values lie in the range of the finite temperature phase transition as for the larger β-values. We conclude that for $\beta = 2.8$ there exists an Aoki phase which however is very small.

4.6 Results for the quark mass

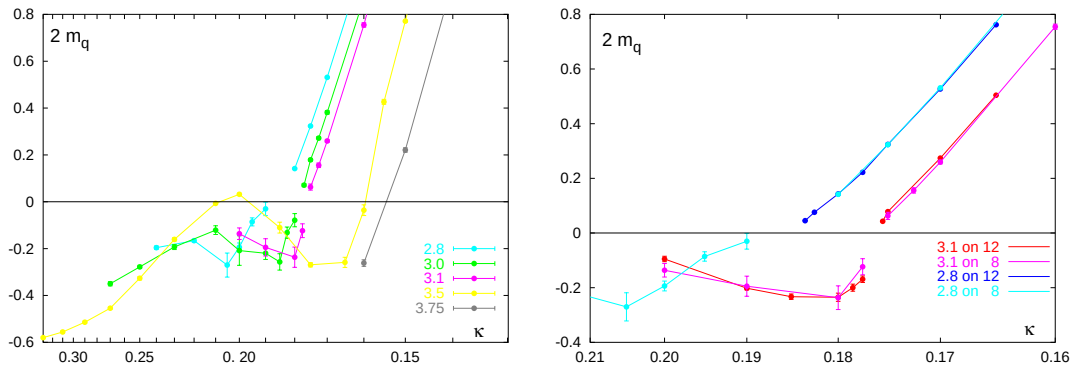

Figure 4.5: Left: Value of the fifth z-slice of the quark mass correlator ratio as a function of $1/\kappa$ for the $8^3 \times 4$ lattice. Right: Fitted quark mass as a function of $1/\kappa$ on the $12^2 \times 24 \times 4$ lattice together with data from the smaller lattice as on the left

As for the pion mass one can only extract the quark mass reliably on the larger lattice. Since the ratio of correlation functions that determine the quark mass is

$\beta =$	2.8	3.0	3.1	3.5	3.75
κ_c	0.1853(3)	0.1823(10)	0.1770(3)	0.1625(25)	0.1550(5)

Table 4.3: Results for the position of the line of vanishing quark mass as extracted from the behaviour of the quark mass correlator ratio.

to be evaluated for large z, one can try to plot the furthest possible point, which on a lattice with periodic boundary conditions is the midpoint. It turns out, that when the data of the smaller lattice are plotted in such a way, there exists again broad agreement with the data from the larger lattice. One can however not take the left plot of Figure 4.5 at face value. Looking at the correlator ratios them self one can quite clearly discern a correlator ratio that will on a larger lattice give a positive quark mass from one that will result in a negative quark mass, see plot one and three of Figure 4.6. But there are also correlator ratios, which we call anomalous, that display positive/negative mass behavior, but whose value at the fifth z-slice is negative/positive, see plot two and four of Figure 4.6. Because of the distinguishable positive/negative mass behaviour we have extracted a location of the critical line defined by the vanishing of the quark mass as the midpoint between the two points between which the behaviour of the quark mass correlator ratio changes, except for $\beta = 2.8$ and 3.1, where a fit could be performed. The results are shown in Table 4.3.

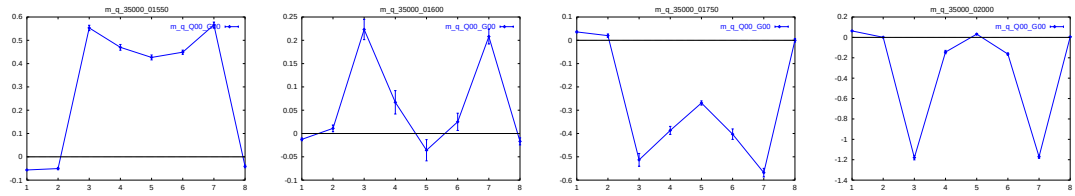

Figure 4.6: From left to right: positive mass correlator ratio, anomalous positive mass correlator ratio, negative mass correlator ratio and anomalous negative mass correlator ratio.

4.7 Results for the chiral condensate

From the measurement of the pion norm and the quark mass we can infer the chiral order parameter. Our results are depicted in Figure 4.7 where the chiral condensate is plotted as a function of the quark mass. This plot gives further evidence that for $\beta = 2.8$ chiral symmetry is broken as the chiral limit is approached. The chiral condensate extrapolates to a nonzero intercept for this β-value. For $\beta = 3.1$ however, the chiral condensates shows a strong curvature, indicating that it will extrapolate to zero in the zero mass limit, as expected when chiral symmetry is restored.

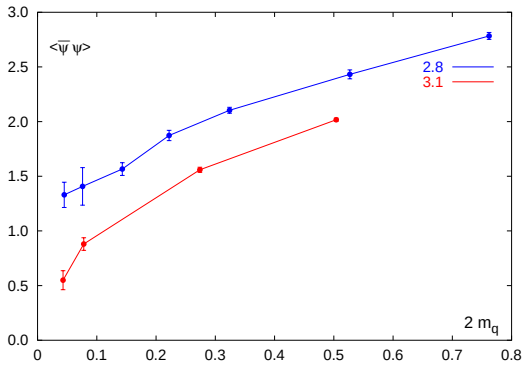

Figure 4.7: Chiral condensate as a function of the quark mass on the $12^2 \times 24 \times 4$ lattice

Chapter 5

Summary

In this study the phase diagram of 2 flavour QCD with dynamical fermions was investigated. For the gauge fields a tree level Symanzik improved action was used. The fermions were simulated in the Wilson formulation also with a tree level Symanzik improved action, which amounts to adding the so called clover term to the standard Wilson action. This system was studied on two different lattice sizes, namely $8^3 \times 4$ and $12^2 \times 24 \times 4$. On the smaller lattice five different β-values were investigated to map out the phase diagram. These were $\beta = 2.8, 3.0, 3.1, 3.5, 3.75$. For each β-value a varying number of κ-values were simulated to find the thermal and critical lines. Once the phase diagram was known the system was simulated on the larger lattice at two β-values $\beta = 2.8$ and 3.1 in the region where the pion was becoming light. For these values, pion and quark masses were extracted and finite volume effects assessed. It was the aim of this study to investigate the following points:

- Does there exist an Aoki phase for the improved Wilson action [18]?
- Does the use of improved actions alleviate problems with strong lattice artifacts found in previous studies [6]?
- What happens to the thermal line once it crosses the line of vanishing quark mass [20]?
- Can one study the finite temperature phase transition with Wilson fermions at light pion masses?

At the smallest β we find evidence for two critical lines, which are very close together and indicate the existence of an Aoki phase for this action. We still find, that the thermal line and the critical line come very close to each other and run almost parallel toward strong coupling. We find no anomalies as for example reported by the MILC collaboration [6]. The strength of the transition decreases with decreasing quark mass as expected. Again at the smallest β-value we find a transition from confined to deconfined behaviour in a regime where the quark mass is negative. This means on the one hand that the thermal line continues past the tip of the cusp of the Aoki phase toward strong coupling and does not turn back toward weak coupling as has been proposed. On the other hand this implies, that the thermal line crosses the critical line, making it possible to study the finite temperature phase transition for light pions.

Outlook and future investigations: There are a number of things, that one would want to elaborate about the phase diagram. The evidence for the existence of an Aoki phase is not very strong and quite indirect. It would be worthwhile to simulate the system at $\beta = 2.8$ for the larger κ-values on the larger lattice to be able to extract the quark mass and establish the existence of a second critical line more precisely. To this end it would also be useful to study the system at even smaller β-values, as the width of the Aoki phase should increase and the signal become clearer. In the light of the discussion in §(2.3) the existence of the Aoki phase for improved Wilson fermions should be established more firmly. Another interesting region is the space between the tip of the cusp and the point where the thermal line crosses the line of vanishing quark mass. Due to the absence of the Aoki phase, the pion should not become massless and one expects a first order transition across the line of vanishing quark mass. This phase transition region will be squeezed out between the cusp of the Aoki phase and the finite temperature transition line in the continuum limit and might therefore be considered unimportant, but it would certainly increase our understanding of the theoretical issues involved in the QCD phase diagram, if the existence of this phenomenon could be established. The next step, of course is the thermodynamics of QCD with improved Wilson fermions. One is interested

how physical observables like pressure and energy density change as a function of temperature. To determine a temperature scale in physical units, one has to do simulations at zero temperature to set the scale. Because it turned out that the simulations were very time consuming with the combination of actions we used, this could not be realized in the present study. Another important direction for future research is the still open question of the order of the phase transition for two massless quarks. Simulations with staggered quarks have so far given puzzling and inconclusive results. The thermodynamics of QCD with Wilson fermions is not very developed and this thesis was meant to change this.

Appendix A

Quantisation of gauge and fermion fields

A.1 Quantising the gauge fields

Lattice Quantum Chromo Dynamics is a non-perturbative implementation of Euclidean field theory using the path integral approach a la Feynman. The finite space time grid serves as a regulator for the theory, that has to be removed as one takes the continuum limit. As one formulates QCD on a lattice one is willing to give up e.g. Lorentz invariance, but what one is not willing to give up is local gauge invariance. This has quite practical reasons, see e.g. reference [24], only gauge invariance guarantees the equality of the quark-gluon, three-gluon and four-gluon couplings and the masslessness of the gluons. To formulate a theory with a local gauge invariance, one uses the concept of covariant derivatives and parallel transporters. A parallel transporter is a mapping from the space of continuous paths on space time into the space of gauge transformations under which our action shall be locally invariant (e.g. U(1),SU(N),...) with the following properties:

$$U(\emptyset) = 1 \tag{A.1}$$

where $\emptyset$ denotes the path with zero length, i.e. $\mathcal{C}_{x,x}$ for all x.

$$U(\mathcal{C}_2 \circ \mathcal{C}_1) = U(\mathcal{C}_2)U(\mathcal{C}_1) \tag{A.2}$$

where $\mathcal{C}_2 \circ \mathcal{C}_1$ denotes the path composed of $\mathcal{C}_1$ followed by $\mathcal{C}_2$.

$$U(-\mathcal{C}) = U(\mathcal{C})^{-1} \tag{A.3}$$

where $-\mathcal{C}$ is the path $\mathcal{C}$ traversed in the opposite way.
Under a local gauge transformation

$$\begin{aligned}\Phi(x) &\to \Phi'(x) = \Lambda^{-1}(x)\Phi(x)\\ \Phi(y) &\to \Phi'(y) = \Lambda^{-1}(y)\Phi(y)\end{aligned} \tag{A.4}$$

a parallel transporter transforms as

$$U(\mathcal{C}_{y,x}) \to U'(\mathcal{C}_{y,x}) = \Lambda^{-1}(y)U(\mathcal{C}_{y,x})\Lambda(x). \tag{A.5}$$

Therefore $U(\mathcal{C}_{y,x})\Phi(x)$ transforms under a gauge transformation like $\Phi(y)$. We can hence compare the field at different points using the covariant distance

$$\Delta_{\mathcal{C}} = U^{-1}(\mathcal{C}_{y,x})\Phi(y) - \Phi(x), \tag{A.6}$$

which depends of course on the specific path $\mathcal{C}_{y,x}$. For the specific paths $\mathcal{C}_\mu(t) = x + \hat{\mu}\cdot t$ we can define the covariant derivative

$$D_\mu\Phi(x) = \lim_{t\to 0}\frac{\Delta_{\mathcal{C}_\mu(t)}\Phi(x)}{t}. \tag{A.7}$$

It is obvious from the above definition, that the covariant derivative transforms under gauge transformations as the field $\Phi(x)$.
If we define the gauge field A_μ as

$$A_\mu(x) = \lim_{t\to 0}\frac{1 - U(\mathcal{C}_\mu(t))}{t}, \tag{A.8}$$

the covariant derivative is given as

$$D_\mu = \partial_\mu + A_\mu(x). \tag{A.9}$$

In order to find the transformation law for the gauge fields, one starts from Equation (A.8) as the defining equation for the infinitesimal generator and uses the gauge transformed parallel transporter. This results in

$$A'_\mu(x) = \Lambda^{-1}(x)A_\mu(x)\Lambda(x) - (\partial_\mu\Lambda(x))\Lambda(x). \tag{A.10}$$

The field strength is defined as the commutator of two covariant derivatives and describes the parallel transport around an infinitesimal parallelogram:

$$F_{\mu\nu} = [D_\mu, D_\nu]\,. \tag{A.11}$$

The continuum action is then given in terms of $F_{\mu\nu}$ as

$$S_G = -\frac{1}{2g^2}\int d^4x \mathrm{Tr} F_{\mu\nu}F^{\mu\nu} \tag{A.12}$$

It is now clear how one can define a gauge invariant action using parallel transporters. In fact given a gauge field, one can reconstruct the parallel transporters via

$$U(\mathcal{C}) = \mathcal{P}\exp\left\{-\int_{\mathcal{C}} A_\mu(x)dx^\mu\right\}, \tag{A.13}$$

where $\mathcal{P}$ denotes path ordering of the gauge fields along $\mathcal{C}$ when evaluating the exponential. It is therefore natural to formulate the gauge dynamics on a lattice in terms of the parallel transporters. On a hypercubic lattice we have to specify the elementary parallel transporters along the links joining two adjacent points in our lattice. They will be denoted $U_\mu(x)$, for further notations see Appendix A. The gauge action on the lattice is formulated in terms of plaquettes, which are the product of link fields around an elementary square in the $\mu-\nu$ plane

$$U_{\mu\nu}(x) = U_\mu(x)U_\nu(x+\hat{\mu})U^\dagger_\mu(x+\hat{\mu}+\hat{\nu})U^\dagger_\nu(x+\hat{\nu}). \tag{A.14}$$

The action is then given as a sum over all plaquettes:

$$S_G = \beta \sum_{x,\mu<\nu} \left(1 - \frac{1}{N}\mathrm{ReTr}U_{\mu\nu}(x)\right) \quad \text{for} SU(N), \tag{A.15}$$

where $\beta = 2N/g^2$. If we expand the above action in powers of the lattice spacing a we get back the continuum action up to terms of $O(a^2)$, see e.g. reference [25]. To fully describe the quantum system one has to specify the measure on the gauge group over which one integrates in the path integral. This measure should respect gauge invariance for the correlation functions resulting from the path integral to be gauge invariant. Fortunately for every compact group G there exists a unique regular Borel probability measure with the desired properties, namely:
1. Normalisation

$$\int_G dU = 1. \tag{A.16}$$

2. Invariance

$$\int_G f(U)dU = \int_G f(UV)dU = \int_G f(VU)dU \quad \text{for all } V \in G. \tag{A.17}$$

Which satisfies

$$\int_G f(U)dU = \int_G f(U^{-1})dU. \tag{A.18}$$

This measure is called the Haar measure of G, for an existence proof see reference [26]. The expectation value of an observable $\mathcal{O}$, which is a function of the gauge field $\{U\}$, is given by

$$\langle \mathcal{O} \rangle = \frac{1}{Z} \int \mathcal{D}U \mathcal{O}(\{U\}) \exp(-S_G(\{U\})) \tag{A.19}$$

$$Z = \int \mathcal{D}U \exp(-S_G(\{U\})) \tag{A.20}$$

$$\mathcal{D}U = \prod_{x,\mu} dU_\mu(x) \tag{A.21}$$

with $dU_\mu(x)$ being the Haar measure for the link from x to $x+\hat{\mu}$.

A.2 Quantising the matter fields

Quantising fermions via the path integral approach is far from trivial. It is indeed nontrivial to see, that the analogy argument, i.e. use Grassmann variables in the path integral instead of ordinary ones, indeed gives the right answer. What we want to show here, is how one can express the trace over a complete set of states in the Fock space of creation and annihilation operators as a functional integral over Grassmann fields. We start from a set of field operators

$$\bar{\chi}^\alpha(x), \chi^\beta(y) \tag{A.22}$$

satisfying canonical commutation relations

$$\left\{\bar{\chi}^\alpha(x), \chi^\beta(y)\right\} = a^3 \gamma_4^{\alpha,\beta} \delta_{x,y}, \tag{A.23}$$

where a is the lattice spacing and x, y are points on a cubic lattice. The vacuum is defined by

$$P_+\chi(x)|0\rangle = \bar{\chi}(x)P_-|0\rangle = 0 \quad \text{with} \quad P_\pm = \frac{1}{2}(1 \pm \gamma_4). \tag{A.24}$$

We also introduce a Grassmann algebra with elements $\psi^\alpha(x), \bar{\psi}^\beta(y)$ with the following anticommutation properties

$$\left\{\psi^\alpha(x), \psi^\beta(y)\right\} = \left\{\bar{\psi}^\alpha(x), \bar{\psi}^\beta(y)\right\} = \left\{\psi^\alpha(x), \bar{\psi}^\beta(y)\right\} = 0. \tag{A.25}$$

These Grassmann fields in turn commute with all creation and annihilation operators. We now define Grassmann coherent states:

$$|\psi, \bar{\psi}\rangle = \exp\left\{a^3 \sum_x [\bar{\chi}(x)P_+\psi(x) + \bar{\psi}(x)P_-\chi(x)]\right\}|0\rangle \tag{A.26}$$

$$\langle\psi, \bar{\psi}| = \langle 0| \exp\left\{a^3 \sum_x [\bar{\psi}(x)P_+\chi(x) + \bar{\chi}(x)P_-\psi(x)]\right\}. \tag{A.27}$$

They are eigenvectors of the creation and annihilation operators with Grassmann eigenvalues, namely:

$$\begin{aligned} P_+\chi(x)|\psi,\bar\psi\rangle &= P_+\psi(x)|\psi,\bar\psi\rangle \\ \bar\chi(x)P_-|\psi,\bar\psi\rangle &= -\bar\psi(x)P_-|\psi,\bar\psi\rangle \\ \langle\psi,\bar\psi|\bar\chi(x)P_+ &= \langle\psi,\bar\psi|\bar\psi(x)P_+ \\ \langle\psi,\bar\psi|P_-\chi(x) &= \langle\psi,\bar\psi| - P_-\psi(x). \end{aligned} \tag{A.28}$$

These states form a complete set in the sense that

$$\mathbf{1} = \int \prod_{\alpha,x}\{a^3 d\bar\psi^\alpha(x) d\psi^\alpha(x)\} \exp\left\{-a^3\sum_{\alpha,x}\bar\psi^\alpha(x)\psi^\alpha(x)\right\} |\psi,\bar\psi\rangle\langle\psi,\bar\psi| \tag{A.29}$$

is a resolution of the identity.
The matrix element of two different coherent states is given by:

$$\langle\psi',\bar\psi'|\psi,\bar\psi\rangle = \exp\left\{a^3\sum_x(\bar\psi(x)'P_+\psi(x) + \bar\psi(x)P_-\psi(x)')\right\}. \tag{A.30}$$

We will now use these results to calculate the partition function

$$\begin{aligned} Z &= \mathrm{Tr}\left\{e^{-\beta\mathcal{H}}\right\} = \sum_n \langle n|\, e^{-\beta\mathcal{H}}\, |n\rangle \\ &= \sum_n \int \prod_{\alpha,x}\{a^3 d\bar\psi^\alpha(x) d\psi^\alpha(x)\} e^{-a^3\sum_x\bar\psi(x)\psi(x)}\, \langle n|\, \psi,\bar\psi\rangle\langle\psi,\bar\psi|e^{-\beta\mathcal{H}}\, |n\rangle \\ &= \sum_n \int \prod_{\alpha,x}\{a^3 d\bar\psi^\alpha(x) d\psi^\alpha(x)\} e^{-a^3\sum_x\bar\psi(x)\psi(x)} \langle\psi,\bar\psi|e^{-\beta\mathcal{H}}\, |n\rangle\, \langle n| - (\psi,\bar\psi)\rangle \\ &= \int \prod_{\alpha,x}\{a^3 d\bar\psi^\alpha(x) d\psi^\alpha(x)\} e^{-a^3\sum_x\bar\psi(x)\psi(x)} \langle\psi,\bar\psi|e^{-\beta\mathcal{H}}| - \psi,\bar\psi\rangle. \end{aligned} \tag{A.31}$$

The minus sign arises from commuting the two Grassmann valued matrix elements past each other. It will give rise to antiperiodic boundary conditions in

time for the Grassmann variables. To proceed from here one splits the time interval into N_τ pieces of length a_0 with $N_\tau a_0 = \beta$ and inserts a complete set of states at each intermediate point.

$$\begin{aligned} Z &= \lim_{N_\tau\to\infty} \mathrm{Tr}\left\{\left(e^{-a_0\mathcal{H}}\right)^N\right\} \\ &= \lim_{N_\tau\to\infty} \int \prod_{t=1}^{N_\tau}\prod_{\alpha,x}\{a^3 d\bar\psi^\alpha(x,t) d\psi^\alpha(x,t)\} e^{-a^3\sum_{x,t}\bar\psi(x,t)\psi(x,t)} \\ &\quad \left\langle\psi,\bar\psi(N_\tau)\right| \exp(-a_0\mathcal{H}) \left|\psi,\bar\psi(N_\tau-1)\right\rangle \cdot \\ &\quad \left\langle\psi,\bar\psi(N_\tau-1)\right| \exp(-a_0\mathcal{H}) \left|\psi,\bar\psi(N_\tau-2)\right\rangle \cdot \ldots \\ &\quad \left\langle\psi,\bar\psi(1)\right| \exp(-a_0\mathcal{H}) \left|-\psi,\bar\psi(N_\tau)\right\rangle \end{aligned} \tag{A.32}$$

The next step is to approximate $\exp(-a_0\mathcal{H})$ by $1-a_0\mathcal{H}$ and evaluate the matrix elements between the coherent states. We must now specify the Hamiltonian. We choose the discretisation introduced by Wilson:

$$\begin{aligned} \mathcal{H} &= \sum_x a^3 \left\{ : \left(\bar\chi(x)\left[m+\frac{3r}{a}\right]\chi(x)\right) : \right. \\ &- \left. \frac{1}{2a}\sum_{k=1}^{3} \bar\chi(x+\hat k)[r+\gamma_k]\chi(x) + \bar\chi(x-\hat k)[r-\gamma_k]\chi(x) \right\}, \end{aligned} \tag{A.33}$$

where :: means normal ordering to subtract the zero point energy:

$$: \bar\chi(x)\chi(x) := \bar\chi(x)P_+\chi(x) - \chi^\alpha(x)(\bar\chi(x)P_-)^\alpha \tag{A.34}$$

From the rules in Equation (A.28) one obtains for the matrix elements of $a_0\mathcal{H}$:

$$\begin{aligned} &\left\langle\psi,\bar\psi(t+1)\right| a_0\mathcal{H} \left|\psi,\bar\psi(t)\right\rangle = \left\langle\psi,\bar\psi(t+1)|\psi,\bar\psi(t)\right\rangle \cdot \\ &\quad a_0\sum_x a^3 \left\{ \left[m+\frac{3r}{a}\right] \left(\bar\psi(x,t+1)P_+\psi(x,t) + \bar\psi(x,t)P_-\psi(x,t+1)\right)\right. \end{aligned}$$

$$-\frac{1}{2a}\sum_{k=1}^{3}(\bar{\psi}(x+\hat{k},t+1)P_{+}+\bar{\psi}(x+\hat{k},t)P_{-})[r+\gamma_k](P_{+}\psi(x,t)+P_{-}\psi(x,t+1))$$
$$+(\bar{\psi}(x-\hat{k},t+1)P_{+}+\bar{\psi}(x-\hat{k},t)P_{-})[r-\gamma_k](P_{+}\psi(x,t)+P_{-}\psi(x,t+1))\Big\} \tag{A.35}$$

Together with Equation (A.30) we then arrive at the following expression for the partition function:

$$\begin{aligned} Z = \lim_{N_\tau\to\infty}\int\prod_{\alpha,x,t}\{a^3 d\bar{\psi}^{\alpha}(x,t)d\psi^{\alpha}(x,t)\}\exp\Big\{ & -a^3 a_0\sum_{x,t}\Big[\frac{1}{a_0}\bar{\psi}(x,t)\psi(x,t) \\ & + \Big[m+\frac{3r}{a}\Big]\big(\bar{\psi}(x,t+1)P_{+}\psi(x,t)+\bar{\psi}(x,t)P_{-}\psi(x,t+1)\big) \\ & - \big(\bar{\psi}(x,t+1)P_{+}\psi(x,t)+\bar{\psi}(x,t-1)P_{-}\psi(x,t)\big) \\ & - \frac{1}{2a}\sum_{k=1}^{3}(\bar{\psi}(x+\hat{k},t+1)P_{+}+\bar{\psi}(x+\hat{k},t)P_{-})[r+\gamma_k](P_{+}\psi(x,t)+P_{-}\psi(x,t+1)) \\ & + (\bar{\psi}(x-\hat{k},t+1)P_{+}+\bar{\psi}(x-\hat{k},t)P_{-})[r-\gamma_k](P_{+}\psi(x,t)+P_{-}\psi(x,t+1))\Big]\Big\} \end{aligned} \tag{A.36}$$

Denoting the points in the four dimensional lattice by x, taking equal lattice spacings in space and time directions $a_0 = a$ and r=1, the integrand can be further simplified to lead to the well known Wilson fermion action, see reference [25]:

$$\begin{aligned} S_f &= \sum_x a^4\Big\{\Big(m+\frac{4}{a}\Big)\bar{\psi}(x)\psi(x) \\ &- \frac{1}{2a}\sum_{\mu=1}^{4}\bar{\psi}(x+\hat{\mu})(1+\gamma_\mu)\psi(x)+\bar{\psi}(x-\hat{\mu})(1-\gamma_\mu)\psi(x)\Big\} \end{aligned} \tag{A.37}$$

This is a discretised version of the free continuum Dirac action. This shows, that to quantise fermions with the path integral approach one starts from the

action and integrates over classical configurations of Grassmann fields, i.e. the analogy argument works. To couple in the gauge fields one has to make the above action gauge invariant. This is achieved by inserting the appropriate parallel transporters. The result is

$$\begin{aligned} S_f &= \sum_x a^4 \Big\{ \left(m + \frac{4}{a}\right) \bar{\psi}(x)\psi(x) \\ &- \frac{1}{2a} \sum_{\mu=1}^{4} \bar{\psi}(x) U_\mu(x)(1-\gamma_\mu)\psi(x+\hat{\mu}) + \bar{\psi}(x) U_\mu^\dagger(x-\hat{\mu})(1+\gamma_\mu)\psi(x-\hat{\mu}) \Big\} \end{aligned} \tag{A.38}$$

Appendix B

Hybrid Monte Carlo equations of motion

This appendix is intended to show the derivation of the equations of motion used in the Hybrid Monte Carlo simulation. We follow reference [22]. In what follows we use the following conventions:

tr	:	colour trace
Tr	:	spinor trace
TR	:	space trace

The derivation starts from the HMC-Hamiltonian

$$\mathcal{H} = \tfrac{1}{2} \sum_{x,\mu} \mathrm{tr}\pi_\mu^2(x) + S_g + \Phi^*(\mathcal{M}^\dagger \mathcal{M})^{-1}\Phi. \tag{B.39}$$

The $\pi_\mu(x)$ are momenta conjugate to the gauge fields $U_\mu(x)$. They live in the group algebra, i.e. are traceless anti-hermitian matrices. The time-evolution of the gauge-fields takes the form

$$\begin{aligned} \dot{U}_\mu(x) &= i\pi_\mu(x)U_\mu(x) \\ \dot{U}_\mu^\dagger(x) &= -iU_\mu^\dagger(x)\pi_\mu(x). \end{aligned} \tag{B.40}$$

The equations of motion for the conjugate momenta are derived from the requirement, that the above Hamiltonian is constant in Molecular-Dynamics-time. It will be shown that the time-derivative of the fermion and gauge contributions to

$\mathcal{H}$ can be written as

$$\dot{\mathcal{S}} = \sum_{x,\mu} \mathrm{tr}[\pi_\mu(x) i F_\mu(x)], \tag{B.41}$$

with

$$F_\mu(x) = G_\mu(x) - G_\mu^\dagger(x). \tag{B.42}$$

The condition of constant energy along the MD-trajectory can therefore be recast into the following:

$$0 = \dot{\mathcal{H}} = \sum_{x,\mu} \mathrm{tr}\{\pi_\mu(x)[\dot{\pi}_\mu(x) + iF_\mu(x)]\}. \tag{B.43}$$

This is zero if $\dot{\pi}_\mu(x)$ is proportional to the unit matrix. To keep $\pi_\mu(x)$ traceless the remaining proportionality constant is chosen as the trace of $F_\mu(x)$. The equations of motion for the conjugate momenta are therefore:

$$i\dot{\pi}_\mu(x) = G_\mu(x) - G_\mu^\dagger(x) - \tfrac{1}{3}\mathrm{tr}\left[G_\mu(x) - G_\mu^\dagger(x)\right]. \tag{B.44}$$

B.1 The gluonic contribution

Spelling out the graphical representation given in Equation (1.20), the gauge action is given by

$$\begin{aligned} S_g &= \beta \sum_{x,\mu>\nu} \frac{5}{3}\left(1 - \frac{1}{2N_c}\mathrm{tr}\left[\mathcal{U}_{\mu\nu}(x) + \mathcal{U}_{\nu\mu}(x)\right]\right) - \\ &\qquad \frac{1}{6}\left(1 - \frac{1}{4N_c}\mathrm{tr}\left[\mathcal{U}_{\mu\nu}^{2\times1}(x) + \mathcal{U}_{\nu\mu}^{1\times2}(x) + \mathcal{U}_{\mu\nu}^{1\times2}(x) + \mathcal{U}_{\nu\mu}^{2\times1}(x)\right]\right), \end{aligned} \tag{B.45}$$

where

$$\mathcal{U}_{\mu,\nu}(x) = U_\mu(x)U_\nu(x+\hat{\mu})U_\mu^\dagger(x+\hat{\nu})U_\nu^\dagger(x)$$

$$\begin{aligned}
\mathcal{U}^{2\times1}_{\mu,\nu}(x) &= U_\mu(x)U_\mu(x+\hat{\mu})U_\nu(x+\hat{\mu}+\hat{\mu})U^\dagger_\mu(x+\hat{\mu}+\hat{\nu})U^\dagger_\mu(x+\hat{\nu})U^\dagger_\nu(x) \\
\mathcal{U}^{1\times2}_{\mu,\nu}(x) &= U_\mu(x)U_\nu(x+\hat{\mu})U_\nu(x+\hat{\mu}+\hat{\nu})U^\dagger_\mu(x+\hat{\nu}+\hat{\nu})U^\dagger_\nu(x+\hat{\nu})U^\dagger_\nu(x).
\end{aligned} \tag{B.46}$$

The first observation is, that one can rewrite the sum over $\mu > \nu$ as a sum over $\mu \neq \nu$ and drop half of the terms. The time derivatives of $\mathcal{U}_{\mu,\nu}(x)$ and $\mathcal{U}^{2\times1}_{\mu\nu}(x)$ are then given by

$$\begin{aligned}
\dot{\mathcal{U}}_{\mu,\nu}(x) &= \dot{U}_\mu(x)U_\nu(x+\hat{\mu})U^\dagger_\mu(x+\hat{\nu})U^\dagger_\nu(x) \\
&+ U_\mu(x)\dot{U}_\nu(x+\hat{\mu})U^\dagger_\mu(x+\hat{\nu})U^\dagger_\nu(x) \\
&+ U_\mu(x)U_\nu(x+\hat{\mu})\dot{U}^\dagger_\mu(x+\hat{\nu})U^\dagger_\nu(x) \\
&+ U_\mu(x)U_\nu(x+\hat{\mu})U^\dagger_\mu(x+\hat{\nu})\dot{U}^\dagger_\nu(x)
\end{aligned} \tag{B.47}$$

$$\begin{aligned}
\dot{\mathcal{U}}^{2\times1}_{\mu,\nu}(x) &= \dot{U}_\mu(x)U_\mu(x+\hat{\mu})U_\nu(x+\hat{\mu}+\hat{\mu})U^\dagger_\mu(x+\hat{\mu}+\hat{\nu})U^\dagger_\mu(x+\hat{\nu})U^\dagger_\nu(x) \\
&\quad U_\mu(x)\dot{U}_\mu(x+\hat{\mu})U_\nu(x+\hat{\mu}+\hat{\mu})U^\dagger_\mu(x+\hat{\mu}+\hat{\nu})U^\dagger_\mu(x+\hat{\nu})U^\dagger_\nu(x) \\
&\quad U_\mu(x)U_\mu(x+\hat{\mu})\dot{U}_\nu(x+\hat{\mu}+\hat{\mu})U^\dagger_\mu(x+\hat{\mu}+\hat{\nu})U^\dagger_\mu(x+\hat{\nu})U^\dagger_\nu(x) \\
&\quad U_\mu(x)U_\mu(x+\hat{\mu})U_\nu(x+\hat{\mu}+\hat{\mu})\dot{U}^\dagger_\mu(x+\hat{\mu}+\hat{\nu})U^\dagger_\mu(x+\hat{\nu})U^\dagger_\nu(x) \\
&\quad U_\mu(x)U_\mu(x+\hat{\mu})U_\nu(x+\hat{\mu}+\hat{\mu})U^\dagger_\mu(x+\hat{\mu}+\hat{\nu})\dot{U}^\dagger_\mu(x+\hat{\nu})U^\dagger_\nu(x) \\
&\quad U_\mu(x)U_\mu(x+\hat{\mu})U_\nu(x+\hat{\mu}+\hat{\mu})U^\dagger_\mu(x+\hat{\mu}+\hat{\nu})U^\dagger_\mu(x+\hat{\nu})\dot{U}^\dagger_\nu(x)
\end{aligned} \tag{B.48}$$

The sum over x and $\mu \neq \nu$ can now be used to change the dummy indices of each term. The cyclic property of the trace can then be used to bring all time derivatives to the front. Finally we make use of Equation (B.40) and write

$$\dot{S}_g = -\frac{\beta}{2N_c}\sum_{x,\mu\neq\nu}\mathrm{tr}\Big[i\pi_\mu(x)U_\mu(x)\frac{5}{3}\Big\{U_\nu(x+\hat{\mu})U^\dagger_\mu(x+\hat{\nu})U^\dagger_\nu(x)$$

$$
\begin{aligned}
& + \; U_\nu^\dagger(x+\hat{\mu}-\hat{\nu})U_\mu^\dagger(x-\hat{\nu})U_\nu(x-\hat{\nu}) - h.c.\Big\} \\
-\frac{1}{12}\mathrm{tr}\Big\{ & \quad U_\mu(x+\hat{\mu})U_\nu(x+\hat{\mu}+\hat{\mu})U_\mu^\dagger(x+\hat{\mu}+\hat{\nu})U_\mu^\dagger(x+\hat{\nu})U_\nu^\dagger(x) \\
& + \; U_\nu(x+\hat{\mu})U_\mu^\dagger(x+\hat{\nu})U_\mu^\dagger(x-\hat{\mu}+\hat{\nu})U_\nu^\dagger(x-\hat{\mu})U_\mu(x-\hat{\mu}) \\
& + \; U_\mu(x+\hat{\mu})U_\nu^\dagger(x+\hat{\mu}+\hat{\mu}-\hat{\nu})U_\mu^\dagger(x+\hat{\mu}-\hat{\nu})U_\mu^\dagger(x-\hat{\nu})U_\nu(x-\hat{\nu}) \\
& + \; U_\nu^\dagger(x+\hat{\mu}-\hat{\nu})U_\mu^\dagger(x-\hat{\nu})U_\mu^\dagger(x-\hat{\mu}-\hat{\nu})U_\nu^\dagger(x-\hat{\mu})U_\mu(x-\hat{\mu}) \\
& + \; U_\nu(x+\hat{\mu})U_\nu(x+\hat{\mu}+\hat{\nu})U_\mu^\dagger(x+\hat{\nu}+\hat{\nu})U_\nu^\dagger(x+\hat{\nu})U_\nu^\dagger(x) \\
& + \; U_\nu^\dagger(x+\hat{\mu}-\nu)U_\nu(x+\hat{\mu}-\hat{\nu}-\hat{\nu})U_\mu^\dagger(x-\hat{\nu}-\hat{\nu})U_\nu(x-\hat{\nu}-\hat{\nu})U_\nu(x-\hat{\nu}) \\
& - \; h.c.\Big\}\Big] \\
= & \sum_{x,\mu} \mathrm{tr}\left\{ i\pi_\mu(x)(G_\mu^G(x) - h.c)\right\} \qquad \text{(B.49)}
\end{aligned}
$$

where the sum over the generalized staples is defined by

$$
\begin{aligned}
G_\mu^G(x) \; = \; & -\frac{\beta}{2N}\sum_{x,\nu\neq\mu} U_\mu(x)\Big[\frac{5}{3}\Big\{U_\nu(x+\hat{\mu})U_\mu^\dagger(x+\hat{\nu})U_\nu^\dagger(x) \\
& \qquad + U_\nu^\dagger(x+\hat{\mu}-\hat{\nu})U_\mu^\dagger(x-\hat{\nu})U_\nu(x-\hat{\nu})\Big\} - \\
& \frac{1}{12}\Big\{U_\mu(x+\hat{\mu})U_\nu(x+\hat{\mu}+\hat{\mu})U_\mu^\dagger(x+\hat{\mu}+\hat{\nu})U_\mu^\dagger(x+\hat{\nu})U_\nu^\dagger(x) \\
& + \; U_\nu(x+\hat{\mu})U_\mu^\dagger(x+\hat{\nu})U_\mu^\dagger(x-\hat{\mu}+\hat{\nu})U_\nu^\dagger(x-\hat{\mu})U_\mu(x-\hat{\mu}) \\
& + \; U_\mu(x+\hat{\mu})U_\nu^\dagger(x+\hat{\mu}+\hat{\mu}-\hat{\nu})U_\mu^\dagger(x+\hat{\mu}-\hat{\nu})U_\mu^\dagger(x-\hat{\nu})U_\nu(x-\hat{\nu}) \\
& + \; U_\nu^\dagger(x+\hat{\mu}-\hat{\nu})U_\mu^\dagger(x-\hat{\nu})U_\mu^\dagger(x-\hat{\mu}-\hat{\nu})U_\nu^\dagger(x-\hat{\mu})U_\mu(x-\hat{\mu}) \\
& + \; U_\nu(x+\hat{\mu})U_\nu(x+\hat{\mu}+\hat{\nu})U_\mu^\dagger(x+\hat{\nu}+\hat{\nu})U_\nu^\dagger(x+\hat{\nu})U_\nu^\dagger(x) \\
& + \; U_\nu^\dagger(x+\hat{\mu}-\nu)U_\nu(x+\hat{\mu}-\hat{\nu}-\hat{\nu})U_\mu^\dagger(x-\hat{\nu}-\hat{\nu})U_\nu(x-\hat{\nu}-\hat{\nu})U_\nu(x-\hat{\nu})\Big\}\Big]
\end{aligned}
\qquad \text{(B.50)}
$$

B.2 The fermionic contribution

In terms of pseudo fermions the fermionic part of the Hamiltonian is given by

$$\mathcal{S}_f = \Phi^*(\mathcal{M}^\dagger\mathcal{M})^{-1}\Phi, \tag{B.51}$$

taking the derivative with respect to time gives

$$\begin{aligned}
\dot{\mathcal{S}}_f &= \Phi^* \cdot \frac{\mathrm{d}}{\mathrm{d}t}(\mathcal{M}^\dagger\mathcal{M})^{-1} \cdot \Phi \\
&= -\Phi^*(\mathcal{M}^\dagger\mathcal{M})^{-1} \cdot \frac{\mathrm{d}}{\mathrm{d}t}(\mathcal{M}^\dagger\mathcal{M}) \cdot (\mathcal{M}^\dagger\mathcal{M})^{-1}\Phi \\
&= -X^* \cdot \frac{\mathrm{d}}{\mathrm{d}t}(\mathcal{M}^\dagger\mathcal{M}) \cdot X \\
&= -X^* \left\{ \frac{\mathrm{d}\mathcal{M}^\dagger}{\mathrm{d}t}\mathcal{M} + \mathcal{M}^\dagger\frac{\mathrm{d}\mathcal{M}}{\mathrm{d}t} \right\} X \\
&= -\mathrm{TR}\ \mathrm{Tr}\ \mathrm{tr} \left\{ \frac{\mathrm{d}\mathcal{M}^\dagger}{\mathrm{d}t}\mathcal{M}\mathcal{P} + \frac{\mathrm{d}\mathcal{M}}{\mathrm{d}t}\mathcal{P}\mathcal{M}^\dagger \right\},
\end{aligned} \tag{B.52}$$

with

$$\begin{aligned}
X(x) &= (\mathcal{M}^\dagger\mathcal{M})^{-1}\Phi(x) \\
\mathcal{P}(x,y) &= X(x) \otimes X^*(y).
\end{aligned} \tag{B.53}$$

We now specify the form of the fermion matrix:

$$\begin{aligned}
\mathcal{M}(x,y) &= \mathcal{A}(x)\delta_{x,y} - \kappa\not{\mathcal{D}}(x,y) \\
\not{\mathcal{D}}(x,y) &= \sum_\mu U_\mu(x)\,(1-\gamma_\mu)\,\delta_{x+\hat{\mu},y} + U_\mu^\dagger(y)\,(1+\gamma_\mu)\,\delta_{x-\hat{\mu},y} \\
\mathcal{A}(x) &= 1 - \frac{i\kappa}{2}c_{SW}\mathcal{F}_{\mu\nu}(x)\sigma_{\mu\nu} \\
\mathcal{F}_{\mu\nu}(x) &= \frac{1}{8i}(\mathcal{Q}_{\mu\nu}(x) - \mathcal{Q}_{\mu\nu}^\dagger(x)) \\
\sigma_{\mu\nu} &= \frac{1}{2}[\gamma_\mu, \gamma_\nu]
\end{aligned}$$

$$\begin{aligned}
\mathcal{Q}_{\mu\nu}(x) &= \mathcal{U}_{\mu,\nu}(x) + \mathcal{U}_{\nu,-\mu}(x) + \mathcal{U}_{-\mu,-\nu}(x) + \mathcal{U}_{-\nu,\mu}(x) \\
\mathcal{U}_{\mu,\nu}(x) &= U_\mu(x) U_\nu(x+\hat{\mu}) U_\mu^\dagger(x+\hat{\nu}) U_\nu^\dagger(x) \\
U_{-\mu}(x) &= U_\mu^\dagger(x-\hat{\mu}) \\
U_{-\mu}^\dagger(x) &= U_\mu(x-\hat{\mu})
\end{aligned} \tag{B.54}$$

Because of the linear structure of the fermion matrix the time derivative of the fermion contribution splits up into two parts, which we will now calculate.

B.2.1 The Wilson term

The first contribution comes from the time derivative of the Wilson term.

$$R1 = \kappa \mathrm{TR}\ \mathrm{Tr}\ \mathrm{tr} \left\{ \dot{\mathcal{D}}^\dagger \mathcal{M} \mathcal{P} + \dot{\mathcal{D}} \mathcal{P} \mathcal{M}^\dagger \right\} \tag{B.55}$$

Note that in the time derivative we have to treat U and $U^\dagger$ as independent degrees of freedom. The contribution at point x is

$$\begin{aligned}
\dot{\not{\mathcal{D}}}(x,y) &= \sum_\mu \dot{U}_\mu(x)\,(1-\gamma_\mu)\,\delta_{x+\hat{\mu},y} + \dot{U}_\mu^\dagger(y)\,(1+\gamma_\mu)\,\delta_{x-\hat{\mu},y} \\
\dot{\not{\mathcal{D}}}^\dagger(x,y) &= \sum_\mu \dot{U}_\mu(x)\,(1+\gamma_\mu)\,\delta_{x+\hat{\mu},y} + \dot{U}_\mu^\dagger(y)\,(1-\gamma_\mu)\,\delta_{x-\hat{\mu},y},
\end{aligned} \tag{B.56}$$

which gives

$$\begin{aligned}
R1 = \kappa \sum_{x,\mu} \mathrm{tr} \Big\{ & \dot{U}_\mu(x)\,(1+\gamma_\mu)\,\mathcal{M}X(x+\hat{\mu}) \otimes X^*(x) \\
+ & \dot{U}_\mu^\dagger(x-\hat{\mu})\,(1-\gamma_\mu)\,\mathcal{M}X(x-\hat{\mu}) \otimes X^*(x) \\
+ & \dot{U}_\mu(x)\,(1-\gamma_\mu)\,X(x+\hat{\mu}) \otimes (\mathcal{M}X)^*(x) \\
+ & \dot{U}_\mu^\dagger(x-\hat{\mu})\,(1+\gamma_\mu)\,X(x-\hat{\mu}) \otimes (\mathcal{M}X)^*(x) \Big\}
\end{aligned} \tag{B.57}$$

and can be rewritten as

$$\begin{aligned} R1 &= \kappa \sum_{x,\mu} \mathrm{tr}\Big\{\dot{U}_\mu(x)\mathrm{Tr}\left[(1+\gamma_\mu)\,\mathcal{M}X(x+\hat{\mu})\otimes X^*(x)\right. \\ &+ \left.(1-\gamma_\mu)\,X(x+\hat{\mu})\otimes X^*\mathcal{M}(x) - h.c.\right]\Big\} \\ &= \sum_{x,\mu} \mathrm{tr}\left\{i\pi_\mu(x)(G^W_\mu(x) - h.c)\right\} \end{aligned} \tag{B.58}$$

with

$$\begin{aligned} G^W_\mu(x) &= \kappa U_\mu(x)\mathrm{Tr}\left[(1+\gamma_\mu)\,\mathcal{M}X(x+\hat{\mu})\otimes X^*(x)\right. \\ &+ \left.(1-\gamma_\mu)\,X(x+\hat{\mu})\otimes X^*\mathcal{M}(x)\right] \end{aligned} \tag{B.59}$$

where we have used Equation (B.40)

B.2.2 The clover term

The second contribution comes from the time derivative of the so called clover term

$$R2 = -\mathrm{TR}\ \mathrm{Tr}\ \mathrm{tr}\left\{\dot{\mathcal{A}}\mathcal{M}\mathcal{P} + \dot{\mathcal{A}}\mathcal{P}\mathcal{M}^\dagger\right\} \tag{B.60}$$

where we have already used the fact that $\mathcal{A}$ is hermitian. Using Equation (B.54) one gets

$$\begin{aligned} R2 &= \mathrm{TR}\ \mathrm{Tr}\ \mathrm{tr}\left\{\frac{i\kappa}{2}c_{SW}\dot{\mathcal{F}}_{\mu\nu}(x)\sigma_{\mu\nu}[\mathcal{M}\mathcal{P} + \mathcal{P}\mathcal{M}^\dagger]\right\} \\ &= \mathrm{TR}\ \mathrm{Tr}\ \mathrm{tr}\left\{\frac{\kappa c_{SW}}{16}\left(\dot{\mathcal{Q}}_{\mu\nu}(x) - \dot{\mathcal{Q}}^\dagger_{\mu\nu}(x)\right)\sigma_{\mu\nu}[\mathcal{M}\mathcal{P} + \mathcal{P}\mathcal{M}^\dagger]\right\} \\ &= \mathrm{TR}\ \mathrm{Tr}\ \mathrm{tr}\left\{\frac{\kappa c_{SW}}{16}\left(\dot{\mathcal{U}}_{\mu,\nu}(x) + \dot{\mathcal{U}}_{\nu,-\mu}(x) + \dot{\mathcal{U}}_{-\mu,-\nu}(x) + \dot{\mathcal{U}}_{-\nu,\mu}(x)\right)\right. \\ &\qquad \left.\sigma_{\mu\nu}[\mathcal{M}\mathcal{P} + \mathcal{P}\mathcal{M}^\dagger] - h.c.\right\} \end{aligned} \tag{B.61}$$

The contribution of the time derivatives at point x is

$$\begin{aligned}
\dot{\mathcal{U}}_{\mu,\nu}(x) &= \dot{U}_\mu(x)U_\nu(x+\hat{\mu})U_\mu^\dagger(x+\hat{\nu})U_\nu^\dagger(x) \\
&+ U_\mu(x)\dot{U}_\nu(x+\hat{\mu})U_\mu^\dagger(x+\hat{\nu})U_\nu^\dagger(x) \\
&+ U_\mu(x)U_\nu(x+\hat{\mu})\dot{U}_\mu^\dagger(x+\hat{\nu})U_\nu^\dagger(x) \\
&+ U_\mu(x)U_\nu(x+\hat{\mu})U_\mu^\dagger(x+\hat{\nu})\dot{U}_\nu^\dagger(x) \qquad \text{(B.62)} \\
\dot{\mathcal{U}}_{\nu,-\mu}(x) &= \dot{U}_\nu(x)U_\mu^\dagger(x-\hat{\mu}+\hat{\nu})U_\nu^\dagger(x-\hat{\mu})U_\mu(x-\hat{\mu}) \\
&+ U_\nu(x)\dot{U}_\mu^\dagger(x-\hat{\mu}+\hat{\nu})U_\nu^\dagger(x-\hat{\mu})U_\mu(x-\hat{\mu}) \\
&+ U_\nu(x)U_\mu^\dagger(x-\hat{\mu}+\hat{\nu})\dot{U}_\nu^\dagger(x-\hat{\mu})U_\mu(x-\hat{\mu}) \\
&+ U_\nu(x)U_\mu^\dagger(x-\hat{\mu}+\hat{\nu})U_\nu^\dagger(x-\hat{\mu})\dot{U}_\mu(x-\hat{\mu}) \qquad \text{(B.63)} \\
\dot{\mathcal{U}}_{-\mu,-\nu}(x) &= \dot{U}_\mu^\dagger(x-\hat{\mu})U_\nu^\dagger(x-\hat{\mu}-\hat{\nu})U_\mu(x-\hat{\mu}-\hat{\nu})U_\nu(x-\hat{\nu}) \\
&+ U_\mu^\dagger(x-\hat{\mu})\dot{U}_\nu^\dagger(x-\hat{\mu}-\hat{\nu})U_\mu(x-\hat{\mu}-\hat{\nu})U_\nu(x-\hat{\nu}) \\
&+ U_\mu^\dagger(x-\hat{\mu})U_\nu^\dagger(x-\hat{\mu}-\hat{\nu})\dot{U}_\mu(x-\hat{\mu}-\hat{\nu})U_\nu(x-\hat{\nu}) \\
&+ U_\mu^\dagger(x-\hat{\mu})U_\nu^\dagger(x-\hat{\mu}-\hat{\nu})U_\mu(x-\hat{\mu}-\hat{\nu})\dot{U}_\nu(x-\hat{\nu}) \qquad \text{(B.64)} \\
\dot{\mathcal{U}}_{-\nu,\mu} &= \dot{U}_\nu^\dagger(x-\hat{\nu})U_\mu(x-\hat{\nu})U_\nu(x+\hat{\mu}-\hat{\nu})U_\mu^\dagger(x) \\
&+ U_\nu^\dagger(x-\hat{\nu})\dot{U}_\mu(x-\hat{\nu})U_\nu(x+\hat{\mu}-\hat{\nu})U_\mu^\dagger(x) \\
&+ U_\nu^\dagger(x-\hat{\nu})U_\mu(x-\hat{\nu})\dot{U}_\nu(x+\hat{\mu}-\hat{\nu})U_\mu^\dagger(x) \\
&+ U_\nu^\dagger(x-\hat{\nu})U_\mu(x-\hat{\nu})U_\nu(x+\hat{\mu}-\hat{\nu})\dot{U}_\mu^\dagger(x) \qquad \text{(B.65)}
\end{aligned}$$

Changing dummy indices one can turn all dotted U fields into $\dot{U}_\mu(x)$, one then uses the cyclicity of the trace to bring $\dot{U}_\mu(x)$ to the front. Those terms containing $\dot{U}_\mu^\dagger(x)$ are exchanged for their hermitian counterparts. As it turns out one half of the remaining terms is equal to the other half, so only 8 different terms are left, leading to

$$\begin{aligned}
R1 &= \frac{\kappa c_{SW}}{8}\sum_{x,\mu}\mathrm{tr}\dot{U}_\mu(x)\Big\{ \\
&\quad U_\nu(x+\hat{\mu})U_\mu^\dagger(x+\hat{\nu})U_\nu^\dagger(x)W_\mu(x,\nu)
\end{aligned}$$

$$
\begin{aligned}
&- U_\nu^\dagger(x+\hat{\mu}-\hat{\nu})U_\mu^\dagger(x-\hat{\nu})U_\nu(x-\hat{\nu})W_\mu(x,\nu) \\
&+ U_\nu(x+\hat{\mu})U_\mu^\dagger(x+\hat{\nu})W_\mu(x+\hat{\nu},\nu)U_\nu^\dagger(x) \\
&- U_\nu^\dagger(x+\hat{\mu}-\hat{\nu})U_\mu^\dagger(x-\hat{\nu})W_\mu(x-\hat{\nu},\nu)U_\nu(x-\hat{\nu}) \\
&+ U_\nu(x+\hat{\mu})W_\mu(x+\hat{\mu}+\hat{\nu},\nu)U_\mu^\dagger(x+\hat{\nu})U_\nu^\dagger(x) \\
&- U_\nu^\dagger(x+\hat{\mu}-\hat{\nu})W_\mu(x+\hat{\mu}-\hat{\nu},\nu)U_\mu^\dagger(x-\hat{\nu})U_\nu(x-\hat{\nu}) \\
&+ W_\mu(x+\hat{\mu},\nu)U_\nu(x+\hat{\mu})U_\mu^\dagger(x+\hat{\nu})U_\nu^\dagger(x) \\
&- W_\mu(x+\hat{\mu},\nu)U_\nu^\dagger(x+\hat{\mu}-\hat{\nu})U_\mu^\dagger(x-\hat{\nu})U_\nu(x+\hat{\nu}) - h.c\Big\} \\
&= \sum_{x,\mu} \mathrm{tr}\left\{i\pi_\mu(x)(G_\mu^C(x) - h.c)\right\} \qquad \text{(B.66)}
\end{aligned}
$$

where we define

$$
W_\mu(x,\nu) = \mathrm{Tr}\left\{\sigma_{\mu,\nu}\left[(\mathcal{M}X)(x)\otimes X^*(x) + X(x)\otimes(\mathcal{M}X)^*(x)\right]\right\}. \qquad \text{(B.67)}
$$

The clover contribution to the force term is hence given by

$$
\begin{aligned}
G_\mu^C(x) &= \frac{\kappa c_{SW}}{8}U_\mu(x)\Big\{ \\
&\quad U_\nu(x+\hat{\mu})U_\mu^\dagger(x+\hat{\nu})U_\nu^\dagger(x)W_\mu(x,\nu) \\
&- U_\nu^\dagger(x+\hat{\mu}-\hat{\nu})U_\mu^\dagger(x-\hat{\nu})U_\nu(x-\hat{\nu})W_\mu(x,\nu) \\
&+ U_\nu(x+\hat{\mu})U_\mu^\dagger(x+\hat{\nu})W_\mu(x+\hat{\nu},\nu)U_\nu^\dagger(x) \\
&- U_\nu^\dagger(x+\hat{\mu}-\hat{\nu})U_\mu^\dagger(x-\hat{\nu})W_\mu(x-\hat{\nu},\nu)U_\nu(x-\hat{\nu}) \\
&+ U_\nu(x+\hat{\mu})W_\mu(x+\hat{\mu}+\hat{\nu},\nu)U_\mu^\dagger(x+\hat{\nu})U_\nu^\dagger(x) \\
&- U_\nu^\dagger(x+\hat{\mu}-\hat{\nu})W_\mu(x+\hat{\mu}-\hat{\nu},\nu)U_\mu^\dagger(x-\hat{\nu})U_\nu(x-\hat{\nu}) \\
&+ W_\mu(x+\hat{\mu},\nu)U_\nu(x+\hat{\mu})U_\mu^\dagger(x+\hat{\nu})U_\nu^\dagger(x) \\
&- W_\mu(x+\hat{\mu},\nu)U_\nu^\dagger(x+\hat{\mu}-\hat{\nu})U_\mu^\dagger(x-\hat{\nu})U_\nu(x+\hat{\nu})\Big\}, \qquad \text{(B.68)}
\end{aligned}
$$

where we have used Equation (B.40) again.

B.3 Putting it all together

In this appendix we have shown the validity of Equation (B.41) and Equation (B.42), with

$$G_\mu(x) = G^G_\mu(x) + G^C_\mu(x) + G^W_\mu(x) \tag{B.69}$$

where $G^G_\mu(x)$, $G^W_\mu(x)$ and $G^C_\mu(x)$ are defined by Equations (B.50), (B.59) and (B.68) respectively. This ends the derivation of the HMC equations of motion.

Appendix C

Tables of Results

In this appendix we collect in tables all the results previously depicted graphically. Each table gives the average values for total action, Polyakov loop, pion norm, pion screening mass, quark mass and the average number of iterations used by the inversion algorithm. For points in the confined phase this was BiCGstab and in the deconfined phase CG.

C.1 Results for the $8^3 \times 4$ lattice

β	κ	action	L	Pion norm	m_π	m_q	# Iterations
2.8000	0.1400	0.9652(9)	0.016(1)	20.55(6)	2.060(5)	2.41(1)	33.24(7)
2.8000	0.1600	0.9564(4)	0.0257(6)	28.99(6)	1.520(5)	1.027(4)	75.6(1)
2.8000	0.1700	0.9477(5)	0.0338(9)	40.3(2)	1.180(7)	0.531(4)	150.6(5)
2.8000	0.1750	0.9410(6)	0.041(1)	52.7(4)	0.976(10)	0.323(4)	251(1)
2.8000	0.1800	0.931(1)	0.050(1)	87(1)	0.679(7)	0.142(3)	530(6)
2.8000	0.1900	0.840(1)	0.053(3)	93(16)	0.50(7)	-0.03(3)	983(34)
2.8000	0.1950	0.812(4)	0.062(3)	59(3)	1.02(4)	-0.09(2)	558(37)
2.8000	0.2000	0.7987(7)	0.052(7)	61(3)	1.22(4)	-0.19(2)	453(8)
2.8000	0.2050	0.789(1)	0.063(2)	53(4)	1.14(5)	-0.27(5)	424(15)
2.8000	0.2200	0.764(1)	0.093(8)	41(1)	1.44(2)	-0.166(6)	325(10)
2.8000	0.2400	0.7363(6)	0.155(3)	30.4(8)	1.50(2)	-0.196(7)	252(5)

Table C.1: Results for $\beta = 2.8$

β	κ	action	L	Pion norm	m_π	m_q	# Iterations
3.0000	0.1200	0.922(2)	0.0148(5)	16.99(1)	2.507(5)	4.53(2)	23.02(2)
3.0000	0.1400	0.9184(4)	0.0176(4)	20.70(2)	2.017(4)	2.268(8)	33.23(3)
3.0000	0.1600	0.9047(5)	0.0290(7)	30.04(6)	1.446(6)	0.868(5)	62.6(1)
3.0000	0.1700	0.894(1)	0.040(2)	44.9(4)	1.03(1)	0.382(8)	123(2)
3.0000	0.1725	0.8869(8)	0.045(1)	52.9(5)	0.919(9)	0.272(7)	230(2)
3.0000	0.1750	0.879(2)	0.051(1)	70(1)	0.779(7)	0.179(6)	192(5)
3.0000	0.1770	0.862(2)	0.056(4)	96(6)	0.59(3)	0.071(7)	517(35)
3.0000	0.1800	0.800(2)	0.075(4)	82(6)	0.53(5)	-0.08(3)	611(27)
3.0000	0.1825	0.775(1)	0.084(6)	48(3)	0.93(6)	-0.13(2)	338(13)
3.0000	0.1850	0.764(2)	0.109(7)	47(5)	1.28(8)	-0.26(3)	275(18)
3.0000	0.1900	0.745(1)	0.111(3)	35(2)	1.51(4)	-0.22(3)	228(6)
3.0000	0.2000	0.731(2)	0.128(3)	31(1)	1.71(5)	-0.21(6)	199(9)
3.0000	0.2100	0.714(2)	0.153(5)	29.2(10)	1.73(4)	-0.12(2)	157(6)
3.0000	0.2300	0.696(1)	0.177(4)	27.5(8)	1.66(3)	-0.19(1)	151(2)
3.0000	0.2500	0.6786(9)	0.209(2)	24.4(2)	1.60(1)	-0.278(7)	155(3)
3.0000	0.2700	0.664(1)	0.235(3)	22.0(8)	1.53(1)	-0.350(9)	160(3)

Table C.2: Results for $\beta = 3.0$

β	κ	action	L	Pion norm	m_π	m_q	# Iterations
3.1000	0.1200	0.8979(6)	0.0149(4)	16.997(10)	2.493(4)	4.40(2)	21.00(1)
3.1000	0.1400	0.8917(6)	0.0189(7)	20.76(3)	1.995(5)	2.17(1)	36.32(5)
3.1000	0.1600	0.8756(8)	0.032(1)	30.5(1)	1.384(7)	0.755(10)	96.5(4)
3.1000	0.1700	0.855(1)	0.046(2)	48.4(7)	0.95(1)	0.260(7)	268(4)
3.1000	0.1725	0.847(1)	0.052(2)	63(2)	0.75(2)	0.156(10)	318(5)
3.1000	0.1750	0.822(1)	0.079(4)	75(5)	0.62(3)	0.06(1)	589(7)
3.1000	0.1775	0.757(1)	0.102(7)	47(3)	1.02(5)	-0.12(3)	334(14)
3.1000	0.1800	0.743(1)	0.115(5)	42(4)	1.22(4)	-0.24(4)	259(18)
3.1000	0.1900	0.7162(7)	0.152(5)	32(1)	1.70(3)	-0.19(4)	162(7)
3.1000	0.2000	0.7022(8)	0.167(2)	30(2)	1.80(6)	-0.14(2)	143(3)

Table C.3: Results for $\beta = 3.1$

β	κ	action	L	Pion norm	m_π	m_q	# Iterations
3.5000	0.1200	0.782(3)	0.0167(7)	17.03(1)	2.395(8)	3.77(3)	25.5(1)
3.5000	0.1400	0.7671(5)	0.026(1)	21.13(3)	1.832(5)	1.57(1)	42.55(6)
3.5000	0.1500	0.748(2)	0.041(3)	25.42(9)	1.444(9)	0.771(6)	71.5(8)
3.5000	0.1550	0.729(2)	0.066(3)	28.5(5)	1.23(1)	0.43(1)	111(14)
3.5000	0.1600	0.6652(7)	0.193(2)	25.9(5)	1.42(3)	-0.04(2)	107(4)
3.5000	0.1650	0.6514(10)	0.205(4)	25.1(3)	1.61(4)	-0.26(2)	92(3)
3.5000	0.1750	0.634(1)	0.228(5)	24.7(3)	1.84(2)	-0.269(9)	77(2)
3.5000	0.1850	0.6210(8)	0.240(3)	22.9(2)	2.00(3)	-0.11(2)	69.0(7)
3.5000	0.2000	0.6086(8)	0.256(5)	22.1(1)	2.09(1)	0.032(5)	68.1(6)
3.5000	0.2100	0.6009(9)	0.264(3)	22.1(3)	2.06(1)	-0.007(4)	68(1)
3.5000	0.2300	0.5900(7)	0.284(4)	20.2(1)	1.946(6)	-0.160(7)	73.5(7)
3.5000	0.2500	0.5802(6)	0.294(2)	19.1(1)	1.819(6)	-0.327(7)	82.9(8)
3.5000	0.2700	0.5732(5)	0.304(3)	17.6(2)	1.744(7)	-0.454(5)	95.2(6)
3.5000	0.2900	0.5668(4)	0.319(2)	16.15(7)	1.697(4)	-0.514(4)	109.2(9)
3.5000	0.3100	0.5614(4)	0.325(1)	14.84(8)	1.681(8)	-0.556(4)	125(1)
3.5000	0.3300	0.5571(3)	0.330(2)	13.51(7)	1.691(3)	-0.580(5)	143.2(6)
3.5000	0.3500	0.5538(3)	0.334(2)	12.38(6)	1.697(5)	-0.605(3)	165.0(6)

Table C.4: Results for $\beta = 3.5$

β	κ	action	L	Pion norm	m_π	m_q	# Iterations
3.7500	0.0800	0.6999(5)	0.0180(5)	13.680(6)	3.474(3)	14.00(3)	2.00(1)
3.7500	0.1000	0.6939(7)	0.0191(6)	14.95(2)	2.902(6)	4.76(4)	5.96(4)
3.7500	0.1100	0.6901(5)	0.021(1)	15.84(2)	2.610(5)	6.89(4)	4.00(1)
3.7500	0.1200	0.6838(6)	0.028(1)	17.03(3)	2.325(5)	3.17(2)	4.86(2)
3.7500	0.1300	0.6735(6)	0.048(3)	18.67(4)	2.014(4)	1.92(1)	19.73(4)
3.7500	0.1400	0.6425(9)	0.162(4)	20.8(1)	1.71(1)	0.94(1)	31.7(3)
3.7500	0.1500	0.616(1)	0.238(6)	22.16(10)	1.60(2)	0.221(10)	66(1)
3.7500	0.1600	0.598(1)	0.252(5)	22.4(1)	1.70(2)	-0.26(1)	66.0(10)

Table C.5: Results for $\beta = 3.75$

C.2 Results for the $12^2 \times 24 \times 4$ lattice

β	κ	action	L	Pion norm	m_π	m_q	# Iterations
2.8000	0.1650	0.9528(3)	0.0281(5)	33.5(3)	1.35(2)	0.762(2)	25.6(1)
2.8000	0.1700	0.9477(4)	0.0340(5)	39.9(5)	1.18(1)	0.527(2)	33.7(1)
2.8000	0.1750	0.9420(2)	0.0393(4)	53.0(5)	0.971(9)	0.324(1)	49.9(2)
2.8000	0.1775	0.9375(3)	0.0433(6)	67(1)	0.83(2)	0.222(1)	66.0(2)
2.8000	0.1800	0.935(1)	0.0458(9)	84(3)	0.69(2)	0.143(1)	94(2)
2.8000	0.1825	0.926(1)	0.0549(7)	139(13)	0.530(7)	0.076(2)	168(2)
2.8000	0.1835	0.9216(5)	0.0539(7)	219(14)	0.42(4)	0.045(1)	244(4)

Table C.6: Results for $\beta = 2.8$

β	κ	action	L	Pion norm	m_π	m_q	# Iterations
3.1000	0.1650	0.8697(5)	0.0348(3)	36.7(2)	1.158(6)	0.504(1)	35.0(1)
3.1000	0.1700	0.8595(9)	0.0433(6)	49.2(6)	0.914(7)	0.274(1)	56.7(4)
3.1000	0.1750	0.8353(8)	0.0621(6)	92(4)	0.559(7)	0.078(2)	129(6)
3.1000	0.1755	0.824(1)	0.0732(8)	104(12)	0.54(4)	0.043(2)	447(14)
3.1000	0.1775	0.7579(4)	0.105(3)	68(13)	0.98(6)	-0.17(1)	382(18)
3.1000	0.1785	0.7504(6)	0.109(1)	44(2)	1.10(2)	-0.20(1)	334(12)
3.1000	0.1800	0.7443(4)	0.111(1)	39(2)	1.29(2)	-0.23(2)	277(9)
3.1000	0.1850	0.7305(3)	0.120(2)	35(1)	1.47(2)	-0.23(1)	196(3)
3.1000	0.1900	0.7195(4)	0.130(1)	32.1(9)	1.54(3)	-0.202(6)	194(9)
3.1000	0.2000	0.7011(3)	0.162(3)	27.7(6)	1.597(6)	-0.10(1)	141(4)

Table C.7: Results for $\beta = 3.1$

References

[1] H. B. Nielsen and M. Ninomiya. Absence of neutrinos on a lattice. 1. proof by homotopy theory. *Nucl. Phys. B*, **185**, 20, (1981).

[2] R.D. Pisarski and F. Wilczek . Remarks on the chiral phase transition in chromodynamics. *Phys. Rev. D*, **29**, 338, (1984).

[3] M. Bochicchio, G. Martinelli, G. Rossi, M. Testa. Chiral symmetry on the lattice with Wilson fermions. *Nucl. Phys. B*, **262**, 331, (1985).

[4] M. Fukugita, S. Ohta, A. Ukawa. Finite-Temperature Behaviour of lattice QCD with Wilson Ferion Action and its Implication on Spectroscopic Studies. *Phys. Rev. Lett.*, **57**, 1974, (1986).

[5] Y. Iwasaki, K. Kanaya, S. Sakai and T. Yoshié. Quark Confinement in Multi-Flavour Quantum-Chromodynamics. *Nucl. Phys. B (Proc. Suppl.)*, **30**, 327, (1993).

[6] C. Bernard, *et al.* Nature of the thermal phase transition with Wilson Quarks. *Phys. Rev. D*, **49**, 3574, (1994).

[7] L.H. Karsten,J. Smit. Lattice fermions:species doubling, chiral invariance, and the triangle anomaly. *Nucl. Phys. B*, **183**, 103, (1981).

[8] K. Symanzik. Cutoff dependence in lattice ϕ^4 theory. In G. 't Hooft, et.al., editor, Recent Developments in gauge theories. Plenum Press, New York, 1980.

[9] M. Lüscher and P. Weisz. On-shell improved lattice gauge theories. *Commun. Math. Phys.*, **97**, 59, (1985).

[10] B. Sheikholeslami and R. Wohlert. Improved Continuum Limit Lattice Action for QCD with Wilson fermions. *Nucl. Phys. B*, **259**, 572, (1985).

[11] Rajan Gupta. Introduction to lattice QCD. hep-lat/9807028.

[12] M. Lüscher and P. Weisz. Computation of the action for on-shell improved lattice gauge theories at weak coupling. *Phys. Lett. B*, **158**, 250, (1985).

[13] N. Kawamoto. Towards the phase structure of Euclidean lattice gauge theories with fermions. *Nucl. Phys. B*, **190**, 617, (1981).

[14] S.Aoki. New Phase sructure for lattice QCD with Wilson fermions. *Phys. Rev. D*, **30**, 2653, (1984).

[15] S. Aoki. Solution to the U(1) Problem on a Lattice. *Phys. Rev. Lett.*, **57**, 3136, (1986).

[16] S. Aoki. U(1) Problem and Lattice QCD. *Nucl. Phys. B*, **314**, 79, (1989).

[17] S. Sharpe, R. Singleton, Jr. Spontaneous Flavor and Parity Breaking with Wilson Fermions. *Phys. Rev. D*, **58**, 074501, (1998).

[18] S. Aoki,A. Ukawa and T. Umemura. Finite-Temperature Phase Structure of Lattice QCD with Wilson Quark action. *Phys. Rev. Lett.*, **76**, 873, (1996).

[19] K. Kanaya. Finite Temperature QCD on the Lattice. *Nucl. Phys. B (Proc. Suppl.)*, **47**, 144, (1996).

[20] M. Creutz. Wilson fermions at finite temperature. *hep-lat/9608024*, (1996).

[21] S. Duane, A. D. Kennedy, B. J. Pendleton, and D. Roweth. Hybrid Monte Carlo. *Phys. Lett. B*, **195**, 216, (1987).

[22] S. Gottlieb, W. Liu, D. Toussaint, R.L. Renken and R.L. Sugar. Hybrid-molecular-dynamics algorithms for the numerical simulation of quantum chromodynamics. *Phys. Rev. D*, **35**, 2531, (1987).

[23] A.D. Kennedy and P. Rossi. Classical mechanics on group manifolds and application to Hybrid Monte Carlo. *Nucl. Phys. B*, **327**, 782, (1989).

[24] G. P. Lepage. Redesigning lattice QCD. In Perturbative and nonperturbative aspects of quantum field theory : Proceedings of the 35. Internationale Universitatswochen fur Kern- und Teilchenphysik, Schladming, Austria, 1997.

[25] I. Montvay and G. Münster. Quantum Fields on a Lattice. Cambridge University Press, Cambridge, 1994.

[26] W. Rudin. Functional Analysis. Tata McGraw-Hill, New Dehli, 1974.